

peptides and glycopeptides, and then both the peptide and sugar chain of each glycopeptide must be analyzed. One of the most effective techniques for mapping proteolytic fragments of glycoproteins is liquid chromatography (LC) coupled with electrospray ionization (ESI) mass spectrometry (MS) (Carr *et al.*, 1993; Duffin *et al.*, 1992; Kawasaki *et al.*, 2004; Ling *et al.*, 1991). The specific detection of glycopeptides can be achieved by monitoring specific diagnostic sugar oxonium ions, such as *m/z* 204 (HexNAc) and 366 (HexHexNAc) produced by cone voltage fragmentation, or by precursor ion scanning (Carr *et al.*, 1993; Duffin *et al.*, 1992). However, when many *N*-glycosylation sites are present within a glycoprotein, the chromatogram becomes extremely complex and assignment of the glycopeptide ions is very difficult.

We present here an alternative strategy for the site-specific glycosylation analysis of a peptide and glycopeptide mixture using LC/ESI MS/MS, where we acquired the product ion spectrum for all significant molecular ions in a data-dependent manner. Product ion spectra of molecular ions allow the specific detection of glycopeptides from a complex mixture of peptides based on the presence of diagnostic sugar oxonium ions of oligosaccharides. Furthermore, this

method allows confirmation of the amino acid sequence of a glycopeptide by the presence of *b*- and *y*-series fragment ions of the peptide. Using this method, we identified one previously unidentified *N*-glycosylated site of ApoB100 and determined the oligosaccharide heterogeneity of each of 17 *N*-glycosylation sites. Our findings provide information on the structure of apoB100 that will be useful to future studies on the structure, function, and metabolism of plasma LDL.

Results

Enzyme digestion

To determine the oligosaccharide heterogeneity at each glycosylation site, reduced and carboxymethylated apoB100 was digested into peptides and glycopeptides. Table I shows the amino acid sequences of the tryptic or chymotryptic peptides, including the putative *N*-glycosylation sites. The putative glycosylation sites were numbered (G1–19). Boldface indicates the previously reported *N*-glycosylation sites (G2–6 and G9–19). When apoB100 is digested by trypsin, potential *N*-glycosylation sites, Asn1341 (G4) and Asn1350 (G5), belong to the same peptide. Because chymotrypsin

Table I. The amino acid sequences of the tryptic or chymotryptic peptides including the putative *N*-glycosylation sites in apoB100

<i>N</i> -glycosylation site ^a		Tryptic digests		Chymotryptic digests	
Residue	ID	Sequence	Theoretical mass ^b	Sequence	Theoretical mass ^b
Asn ⁷	G1	EEEMLEN ⁷ VSLVCPK	1677.8	EN ⁷ VSL	560.3
Asn ¹⁵⁸	G2	QVFLD ¹⁵⁸ TVYGN ¹⁵⁸ CSTHFTVK	2229.1	GN ¹⁵⁸ CSTHF	822.3
Asn ⁹⁵⁶	G3	QVFPGLNYCTSGAYSN ⁹⁵⁶ ASSTDSASYPLTGDR	3550.5	SN ⁹⁵⁶ ASSTDSASY	1088.4
Asn ¹³⁴¹	G4	LYQLQVLLGVLDLSTNVYSNLYN ¹³⁴¹	4692.3	N ¹³⁴¹ W	318.1
Asn ¹³⁵⁰	G5	WSASYSGGN ¹³⁵⁰ TSTDHFSLR	4692.3	SGGN ¹³⁵⁰ TSTDHF	1021.4
Asn ¹⁴⁹⁶	G6	FN ¹⁴⁹⁶ SSYLQGTNQITGR	1684.8	N ¹⁴⁹⁶ SSY	469.2
Asn ²²¹²	G7	TIHDLHLFIENIDFN ²²¹² K	1968.0	N ²²¹² KSGSSTASW	1023.5
Asn ²⁵³³	G8	N ²⁵³³ LTDFAEQYSIQDWAK	1928.9	AAKN ²⁵³³ L	515.3
Asn ²⁷⁵²	G9	IQSPLFLDANADIGN ²⁷⁵² GTTSANEAGIAASITAK	3231.6	DANADIGN ²⁷⁵² GTTSANEAGIAASITAKGESKL	2846.4
Asn ²⁹⁵⁵	G10	VNQNLVYESGSLN ²⁹⁵⁵ FSK	1797.9	N ²⁹⁵⁵ F	279.1
Asn ³⁰⁷⁴	G11	YNQN ³⁰⁷⁴ FSAGNNENIMEAHVINGEANLD FLNIPLTIPEMR	4359.1	NQN ³⁰⁷⁴ F	521.2
Asn ³¹⁹⁷	G12	SYN ³¹⁹⁷ ETK	740.3	N ³¹⁹⁷ ETKIKF	878.5
Asn ³³⁰⁹	G13	ELCTISHIFIPAMGN ³³⁰⁹ ITYDFSEK	2704.3	IPAMGN ³³⁰⁹ ITY	978.5
Asn ³³³¹	G14	SSVITLNTNAELFN ³³³¹ QSDIVAHLLSSSSVIDALQYK	3864.0	N ³³³¹ QSDIV AHL	995.5
Asn ³³⁸⁴	G15	FVEGSHN ³³⁸⁴ STVSLTTK	1605.8	VEGSHN ³³⁸⁴ STVSL	1128.5
Asn ³⁴³⁸	G16	YDFN ³⁴³⁸ SSMLYSTAK	1525.7	N ³⁴³⁸ SSML	550.2
Asn ³⁸⁶⁸	G17	FEVDS ³⁸⁶⁸ PVYN ³⁸⁶⁸ ATWSASLK	1912.9	N ³⁸⁶⁸ ATW	490.2
Asn ⁴²¹⁰	G18	VHN ⁴²¹⁰ GSEILFSYFQDLVITLPFELR	2836.5	SKVHN ⁴²¹⁰ GSEIL	1082.6
Asn ⁴⁴⁰⁴	G19	DFHSEYIVSASN ⁴⁴⁰⁴ FTSQLSSQVEQFLHR	3155.5	IVSASN ⁴⁴⁰⁴ F	736.4

Human apoB100 amino acid sequence (NP_000375, apolipoprotein B [gi:4502153]) was obtained from the NCBI database (www.ncbi.nlm.nih.gov/pubmed). Boldface indicates previously reported *N*-glycosylation sites. Cysteine residue was carboxymethylated, and carboxymethylated cysteine was underscored.

^aPotential *N*-glycosylation sites were identified with the consensus sequence NXS/T, where X is any amino acid except P.

^bMonoisotopic mass value.

can cleave apoB100 into glycopeptides containing one glycosylation site, we attempted to analyze both proteolytic fragments from trypsin digestion and chymotrypsin digestion to identify the site-specific glycosylation.

LC/ESI MS/MS analysis of tryptic digest of apoB100

The schema of a site-specific glycosylation analysis of apoB100 is shown in Figure 1. A mixture of peptides and glycopeptides was subjected to LC/ESI MS/MS with a reversed-phase column. Figure 2A shows a total ion chromatogram (TIC) of a time-of-flight (TOF) MS scan for the full scan m/z 1000–2000. When double or higher charged molecular ions were detected, the product ion spectrum was automatically acquired. Figure 2B shows a TIC of the product ion scan. The collision energy at the second quadrupole for the product ion scan was adjusted from 50 to 80 eV depending on the size and charge of the precursor ion. Under these conditions, peptide precursor ions produced b- and y-series fragment ions derived from its amino acid sequence (data not shown), and glycopeptide precursor ions produced abundant carbohydrate-specific ions, m/z 204, 186, 168, and 366 (described later). The intensity of ions at m/z 204.05–204.15 (HexNAc, 204.08) in each product ion scan are illustrated in Figure 2C. The extracted ion chromatogram at m/z 204 (Figure 2C) and 366 (data not shown) provides useful information on the selection of glycopeptide precursor ions. The product ion spectra of glycopeptides show a very characteristic pattern (see later figures). There were intense oligosaccharide-derived peaks of m/z 204 (HexNAc), 366 (HexHexNAc), 186 (HexNAc-H₂O), and 168 (HexNAc-2H₂O), and if present, 163 (Hex), 292 (Neu5Ac), and 274 (Neu5Ac-H₂O). Therefore, we can very easily distinguish the glycopeptide precursor ions from peptide ions. As expected, many parent ions having 204 and

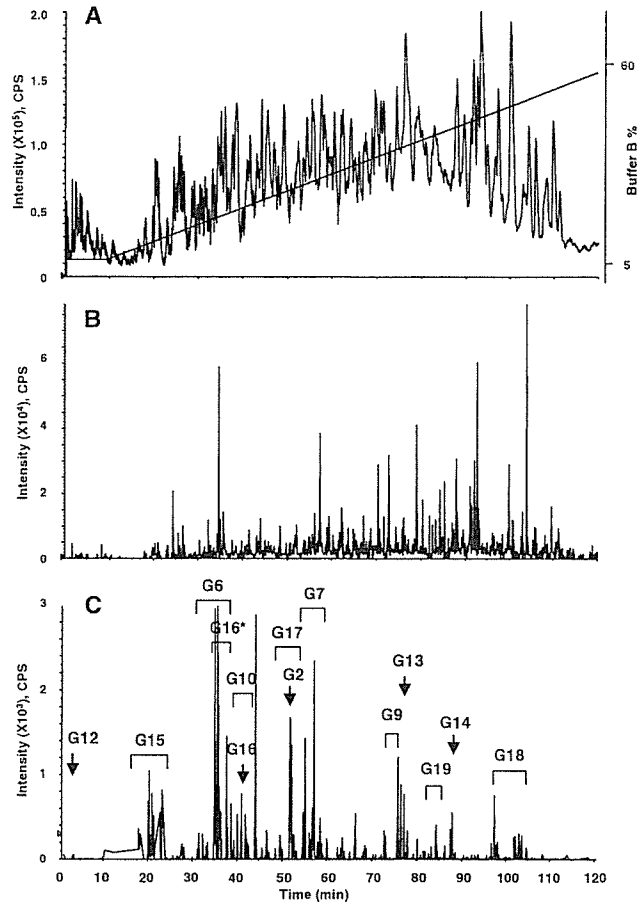


Fig. 2. LC/ESI MS/MS of tryptic digest of apolipoprotein B100. TIC of the TOF MS scan for the full scan m/z 1000–2000 and the HPLC gradient are indicated (A). TIC of the product ion scan data-dependently acquired (B). Extract ion chromatogram at m/z 204 of product ion spectra (C). Arrows and brackets denote glycopeptide fraction and *N*-glycosylation site ID. G16* was found to be oxidized at a methionine residue.

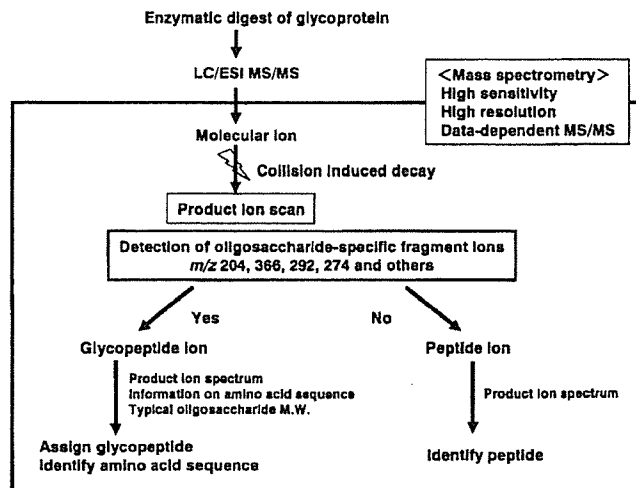


Fig. 1. Schema of site-specific glycosylation analysis. Glycoprotein was digested into peptides and glycopeptides containing only one glycosylation site. Only LC/ESI MS/MS was used. Data-dependent MS/MS acquisition was used to differentiate glycopeptide ions from peptide ions and identify the amino acid sequence of the glycopeptides. The oligosaccharide structure was deduced based on the calculated oligosaccharide molecular weight.

366 fragment ions in the product ion spectrum were detected, and most of these precursor ions were found as glycopeptides.

The glycopeptides were assigned based on an examination of product ion spectra using the information on the peptides containing a putative *N*-glycosylation site. Figures 3A, 3B, and 3C show the product ion spectra of 1412.1 (+2) at 18 min, 1160.4 (+3) at 20 min and 1271.1 (+3) at 22 min for the glycopeptides. There were intense carbohydrate B⁺ ions such as m/z 204 (HexNAc), 366 (HexHexNAc), and 186 (HexNAc-H₂O) and other weak peaks in the product ion spectra. These product ion spectra were very similar to each other (Figure 3A, 3B, and 3C). Careful examination of these product ion spectra for the glycopeptides revealed that several fragment ions were consistent with b- and y-series fragment ions derived from the peptide FVEGSHNSTVSLTTK (residue 3378–3392). The deduced b- and y-series fragment ions of the peptide FVEGSHNSTVSLTTK were listed, and the fragment ions detected in the product ion spectrum of 1160.4 (+3) are underscored in the table (Figure 3D). The molecular ions of the peptide (m/z 1606) and

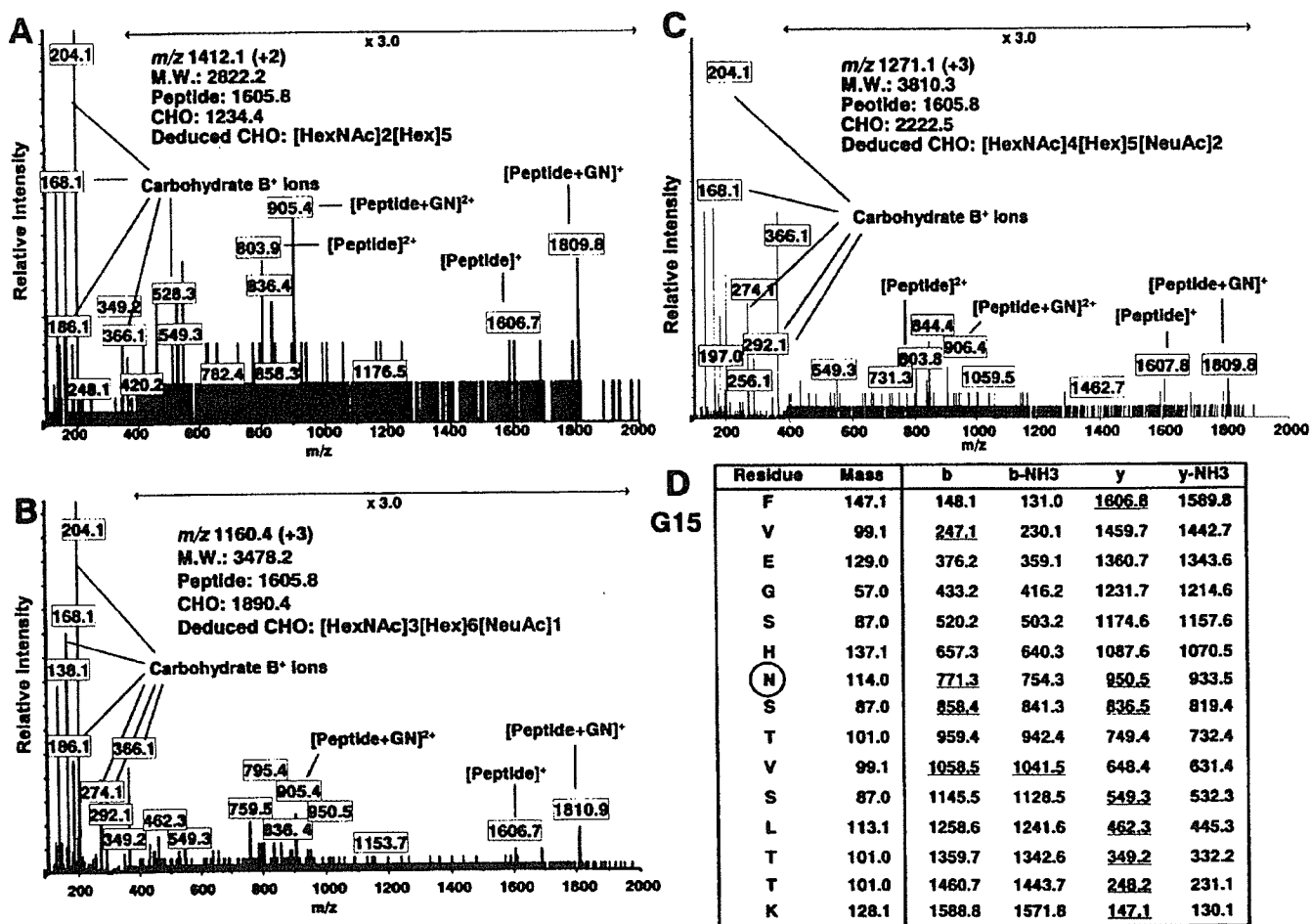


Fig. 3. Product ion spectra of the *N*-glycosylated peptides containing Asn3384 (G15). Product ion scan of m/z 1412.1 (+2) (A), 1160.4 (+3) (B), and 1271.1 (+3) (C) at 18, 20, and 22 min, respectively. These spectra show a characteristic fragmentation pattern with abundant carbohydrate-diagnostic oxonium ions at 163, 168, 186, 204, and 366 and very similar patterns to each other. The oxonium ions at m/z 292 (Neu5Ac) and 274 (Neu5A-H₂O) were observed in the peptides having sialylated oligosaccharide (B) and (C). Several fragment ions are consistent with the b- and y-series fragment ions derived from the peptide FVEGSHNSTVSLTTK (residue 3378–3392). [Peptide]⁺ and [peptide+GlcNAc]⁺ ions were also detected. (D) shows m/z of the proposed b- and y-series fragment ions of the peptide and the fragment ions detected in Figure 3B are underscored. Based on the calculated oligosaccharide mass, the deduced oligosaccharide structure was presented. GN, *N*-acetylglucosamine.

peptide + GlcNAc (m/z 1809) were also detected in the product ion spectra (Figure 3A, 3B, and 3C). These results suggest that these glycopeptides have the same peptide, FVEGSHNSTVSLTTK, including the *N*-glycosylation site Asn3384 (G15). Carbohydrate molecular weight was calculated by subtracting the theoretical molecular weight of the peptide (1605.8) from the calculated molecular weight of the glycopeptide and adding the molecular weight of H₂O (18.0). The oligosaccharide structure was deduced based on the molecular weight and previously reported oligosaccharides of apoB100. The presence of product ions at m/z 274 (Neu5Ac-H₂O) and 292 (Neu5Ac) suggested that those at m/z 1160.4 (+3) and 1271.1 (+3) were glycopeptide ions having sialylated oligosaccharides. Thus the carbohydrate compositions, [HexNAc]₂[Hex]₅, [HexNAc]₃[Hex]₆[Neu5Ac]₁, and [HexNAc]₄[Hex]₅[Neu5Ac]₂, were deduced from the carbohydrate molecular weights, 1234.4, 1890.4, and 2222.5, respectively.

Figures 4 shows the product ion spectra of 1294.8 (+3) at 55 min and 1152.7 (+3) at 35 min for other glycopeptides. There are intense carbohydrate B⁺ ions in the product ion spectra. Several ions consisting of b- and y-series fragment ions from the peptide TIHDLHLFIENIDHNK (residue 2198–2213) were found in the product ion spectrum of 1294.8 (+3) (Figure 4A), and detected ions are underscored in the table. The molecular ions of the peptide (m/z 1968.9) were also detected in the product ion spectra. The carbohydrate molecular weight was calculated from the molecular weight of the peptide, 1968.0, and the molecular weight of the glycopeptide, 3881.4. Carbohydrate composition was deduced from the carbohydrate molecular weight (1931.4) and presence of Neu5Ac. Thus, the peptide moiety TIHDLHLFIENIDHNK and carbohydrate composition [HexNAc]₄[Hex]₅[Neu5Ac]₁ were suggested.

Many ions in the product ion spectrum of 1152.7 (+3) were consistent with the b- and y-series fragment ions

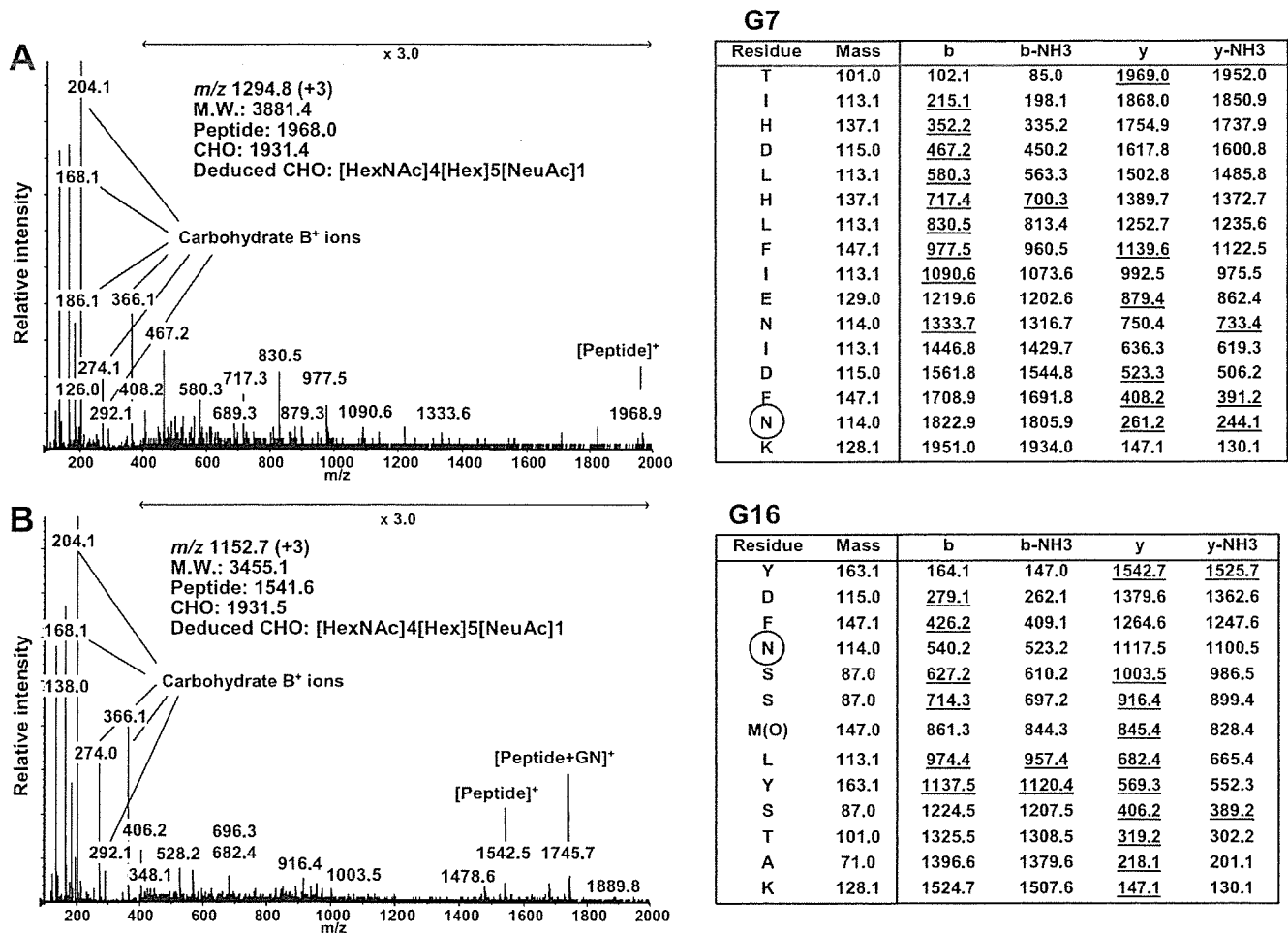


Fig. 4. Product ion spectra of the tryptic *N*-glycosylated peptides of apoB100. (A) Product ion spectrum of m/z 1294.8 (+3) at 55 min for the glycopeptide containing Asn2212 (G7). Several ions are consistent with the b- and y-series fragment ions derived from the peptide TIHDLHLFIENIDFNK (residue 2198–2213). Table shows m/z of the proposed b- and y-series fragment ions and the detected ions are underscored. (B) Product ion spectrum of m/z 1152.7 (+3) at 35 min for the glycopeptide containing Asn3438 (G16) with oxidized methionine. The methionine residue at 3441 was considered oxidized. Several ions are consistent with the b- and y-series fragment ions derived from the peptide YDFNSSM(O)LYSTAK (residue 3435–3447). Table shows m/z of the proposed b- and y-series fragment ions and the detected ions are underscored. M(O), oxidized methionine.

derived from the peptide YSFNSSMLYSTAK (Figure 4B). However, the deduced peptide ion m/z at 1526.7 and peptide + GlcNAc at 1729.8 were not detected. The difference of 203 between the product ions at m/z 1542.5 and 1745.7 suggests that the molecular weight of the peptide moiety may be 1541.5, and an increase in mass of 16 Da suggests that the methionine residue of YSFNSSMLYSTAK (residue 3435–3447, molecular weight 1525.7) was oxidized. The deduced b- and y-series fragment ions of the peptide, YSFNSSMLYSTAK, with the oxidized methionine are listed and detected peptide fragment ions are underscored. Thus, the product ions at m/z 1542.5 and 1745.7 were considered the peptide and peptide + GlcNAc ions, respectively. Our method identified unexpected oxidation of methionine residue (Figure 4B). The carbohydrate molecular weight was calculated, and the carbohydrate composition, [HexNAc]₄[Hex]₅[Neu5Ac]₁, was deduced from the carbohydrate molecular weight, 1931.4, and presence of Neu5Ac.

Results of site-specific glycosylation analysis from tryptic digest are summarized in Table II. To avoid misassignment, only ions that were confirmed as glycopeptides by the product ion spectra or coeluting ions with glycopeptides were listed. We determined 13 of the 19 potential *N*-glycosylation sites and the oligosaccharide heterogeneity at each site in a site-specific glycosylation analysis of the tryptic digest of apoB100. The type of oligosaccharide was deduced based on the oligosaccharide composition. Glycopeptides containing *N*-glycosylation sites Asn7, 956, 1341, 1350, 2533, and 3074 (G1, 3, 4, 5, 8, and 11) could not be detected. The relative peak intensity does not accurately express the relative amount of glycoforms, because of the different ionization efficiency of each glycoform, different detection sensitivity at m/z , and simultaneous acquisition of MS and MS/MS spectra. However, the relative peak intensity of each glycopeptide would provide an indication of the distribution in glycoforms.

Table II. Site-specific glycosylation analysis of the tryptic digest of apoB100 using LC/ESI MS/MS

Glycosylation site ID	Retention time (min)	Peptide theoretical MW ^a	Glycopeptides			Oligosaccharide			Deduced Type ^e	
			<i>m/z</i>	Charge	Calculated MW ^a	Calculated MW ^a	Theoretical MW ^a	Relative peak intensity (%) ^b		Composition ^c
G1	—	1677.8	—	—	—	—	—	—	—	
G2	51	2229.1	1365.6	+3	4093.8	1882.7	1882.6	7	[HexNAc]2[Hex]9	High mannose
	51	2229.1	1311.6	+3	3931.7	1720.6	1720.6	13	[HexNAc]2[Hex]8	High mannose
	51	2229.1	1257.5	+3	3769.5	1558.4	1558.5	22	[HexNAc]2[Hex]7	High mannose
	51	2229.1	1203.5	+3	3607.6	1396.6	1396.5	13	[HexNAc]2[Hex]6	High mannose
	51	2229.1	1149.5	+3	3445.5	1234.4	1234.4	100	[HexNAc]2[Hex]5	High mannose
	51	2229.1	1723.7	+2	3445.4	1234.4	—	—	—	—
G3	—	3550.5	—	—	—	—	—	—	—	
G4, G5	—	4692.3	—	—	—	—	—	—	—	
G6	33	1684.8	1451.6	+2	2901.2	1234.4	1234.4	15	[HexNAc]2[Hex]5	High mannose
	34	1684.8	1200.4	+3	3598.2	1931.4	1931.7	100	[HexNAc]4[Hex]5[Neu5Ac]1	Biantennary complex
	34	1684.8	1800.1	+2	3598.2	1931.4	—	—	—	—
	35	1684.8	1146.4	+3	3436.2	1769.4	1769.6	23	[HexNAc]4[Hex]4[Neu5Ac]1	Biantennary complex
	35	1684.8	1719.2	+2	3436.4	1769.6	—	—	—	—
	35	1684.8	1078.7	+3	3233.1	1566.3	1566.6	11	[HexNAc]3[Hex]4[Neu5Ac]1	Monoantennary complex
	35	1684.8	1132.8	+3	3395.4	1728.6	1728.6	5	[HexNAc]3[Hex]5[Neu5Ac]1	Hybrid
	35	1684.8	1186.8	+3	3557.4	1890.6	1890.7	3	[HexNAc]3[Hex]6[Neu5Ac]1	Hybrid
	35	1684.8	1240.8	+3	3719.4	2052.6	2052.7	3	[HexNAc]3[Hex]7[Neu5Ac]1	Hybrid
	37	1684.8	1297.4	+3	3889.2	2222.4	2222.8	24	[HexNAc]4[Hex]5[Neu5Ac]2	Biantennary complex
G7	37	1684.8	1945.7	+2	3889.4	2222.6	—	—	—	—
	54	1968.0	1294.8	+3	3881.4	1931.4	1931.7	66	[HexNAc]4[Hex]5[Neu5Ac]1	Biantennary complex
	58	1968.0	1044.2	+4	4172.8	2222.8	2222.8	100	[HexNAc]4[Hex]5[Neu5Ac]2	Biantennary complex
	58	1968.0	1391.9	+3	4172.7	2222.7	—	—	—	—
G8	—	1928.9	—	—	—	—	—	—	—	
G9	73	3231.6	1360.4	+4	5437.6	2224.0	2222.8	—	[HexNAc]4[Hex]5[Neu5Ac]2	Biantennary complex
	40	1797.9	1238.1	+3	3711.3	1931.4	1931.7	41	[HexNAc]4[Hex]5[Neu5Ac]1	Biantennary complex
G10	41	1797.9	1856.7	+2	3711.4	1931.5	—	—	—	—

Table II. continued

Glycosylation site ID	Retention time (min)	Peptide theoretical MW ^a	Glycopeptides			Oligosaccharide			Relative peak intensity (%) ^b	Composition ^c	Deduced Type ^c
			m/z	Charge	Calculated MW ^a	Calculated MW ^a	Theoretical MW ^a				
G11	43	1797.9	1001.6	+4	4002.4	2222.5	2222.8	100	[HexNAc]4[Hex]5[Neu5Ac]2	Biantennary complex	
	43	1797.9	1335.1	+3	4002.3	2222.4	—	—	—	—	
	—	4359.1	—	—	—	—	—	—	—	—	
G12	2	740.3	1473.6	+2	2945.2	2222.9	2222.8	—	[HexNAc]4[Hex]5[Neu5Ac]2	Biantennary complex	
	75	2704.3	1102.7	+4	4406.8	1720.5	1720.6	22	[HexNAc]2[Hex]8	High mannose	
G13	75	2704.3	1470.0	+3	4406.9	1720.6	1558.5	54	[HexNAc]2[Hex]7	High mannose	
	76	2704.3	1062.2	+4	4244.8	1558.5	1558.4	—	—	—	
	76	2704.3	1415.9	+3	4244.7	1558.4	1396.5	100	[HexNAc]2[Hex]6	High mannose	
	76	2704.3	1021.6	+4	4082.4	1396.1	1234.4	50	[HexNAc]2[Hex]5	High mannose	
	76	2704.3	1361.9	+3	4082.7	1396.4	1882.6	—	[HexNAc]2[Hex]9	High mannose	
	76	2704.3	1307.9	+3	3920.7	1234.4	1882.7	—	—	—	
	88	3864.0	1146.7	+5	5728.7	1882.7	1882.3	—	—	—	
	88	3864.0	1433.1	+4	5728.3	1882.3	1599.6	8	[HexNAc]3[Hex]6	Hybrid	
	17	1605.8	1063.4	+3	3187.2	1599.4	1640.6	20	[HexNAc]4[Hex]5	Biantennary complex	
	17	1605.8	1077.0	+3	3228.0	1640.2	1437.5	20	[HexNAc]3[Hex]5	Hybrid	
G14	17	1605.8	1009.4	+3	3025.2	1437.4	1478.2	13	[HexNAc]4[Hex]4	Biantennary complex	
	18	1605.8	1513.6	+2	3025.3	1437.5	1234.4	4	[HexNAc]2[Hex]5	High mannose	
	18	1605.8	1023.0	+3	3066.0	1478.2	1931.7	100	[HexNAc]4[Hex]5[Neu5Ac]1	Biantennary complex	
	18	1605.8	1412.1	+2	2822.2	1234.4	1890.7	10	[HexNAc]3[Hex]6[Neu5Ac]1	Hybrid	
	20	1605.8	1174.1	+3	3519.3	1931.5	1728.6	94	[HexNAc]3[Hex]5[Neu5Ac]1	Hybrid	
	20	1605.8	1760.7	+2	3519.4	1931.6	—	—	—	—	
	20	1605.8	1160.4	+3	3478.2	1890.4	2077.7	4	[HexNAc]4[Hex]5[Neu5Ac]1[Fuc]1	Biantennary complex	
	20	1605.8	1106.4	+3	3316.2	1728.4	1566.6	42	[HexNAc]3[Hex]4[Neu5Ac]1	Monoantennary complex	
	20	1605.8	1659.2	+2	3316.4	1728.6	1566.6	—	—	—	
	20	1605.8	1222.8	+3	3665.4	2077.6	1769.6	23	[HexNAc]4[Hex]4[Neu5Ac]1	Biantennary complex	
G15	20	1605.8	1052.4	+3	3154.2	1566.4	2222.8	49	[HexNAc]4[Hex]5[Neu5Ac]2	Biantennary complex	
	20	1605.8	1578.2	+2	3154.4	1566.6	1931.7	—	[HexNAc]4[Hex]5[Neu5Ac]1	Biantennary complex	
	21	1605.8	1120.0	+3	3357.0	1769.2	1931.6	100	[HexNAc]4[Hex]5[Neu5Ac]1	Biantennary complex	
	22	1605.8	1271.1	+3	3810.3	2222.5	1931.7	—	—	—	
	42	1525.7	1147.4	+3	3439.2	1931.5	1931.6	—	—	—	
	42	1525.7	1720.7	+2	3439.3	1931.6	1931.7	—	—	—	
	35	1541.7*	1152.7	+3	3455.1	1931.4	1931.7	100	[HexNAc]4[Hex]5[Neu5Ac]1	Biantennary complex	

Table II. continued

Glycosylation site ID	Retention time (min)	Peptide theoretical MW ^a	Glycopeptides			Oligosaccharide			Deduced Type ^c	
			<i>m/z</i>	Charge	Calculated MW ^a	Theoretical MW ^a	Relative peak intensity (%) ^b	Composition ^c		
G17	35	1541.7*	1728.6	+2	3455.2	1931.5	1769.6	9	[HexNAc]4[Hex]4[Neu5Ac]1	Biantennary complex
	36	1541.7*	1098.7	+3	3293.1	1769.4	1769.5	18	[HexNAc]3[Hex]4[Neu5Ac]1	Monoantennary complex
	36	1541.7*	1647.6	+2	3293.2	1769.5	1566.6	19	[HexNAc]4[Hex]5[Neu5Ac]2	Biantennary complex
	36	1541.7*	1546.1	+2	3090.2	1566.5	2222.8	100	[HexNAc]4[Hex]5[Neu5Ac]1	Biantennary complex
	38	1541.7*	1249.8	+3	3746.4	2222.7	1931.7	6	[HexNAc]5[Hex]6[Neu5Ac]2	Triantennary complex
	51	1912.9	1276.5	+3	3826.5	1931.6	2222.7	39	[HexNAc]4[Hex]5[Neu5Ac]2	Biantennary complex
	51	1912.9	1914.3	+2	3826.6	1931.7	2222.6	100	[HexNAc]4[Hex]5[Neu5Ac]1	Biantennary complex
	54	1912.9	1495.3	+3	4482.9	2588.0	1931.7	10	[HexNAc]4[Hex]4[Neu5Ac]1	Biantennary complex
	54	1912.9	1030.4	+4	4117.6	2222.7	2222.8	64	[HexNAc]4[Hex]5[Neu5Ac]2	Biantennary complex
	54	1912.9	1373.5	+3	4117.5	2222.6	1931.7	79	[HexNAc]4[Hex]5[Neu5Ac]1	Biantennary complex
G18	98	2836.5	1188.5	+4	4750.2	1931.7	1769.6	10	[HexNAc]4[Hex]4[Neu5Ac]1	Biantennary complex
	98	2836.5	1584.4	+3	4750.1	1931.7	2222.8	64	[HexNAc]4[Hex]5[Neu5Ac]2	Biantennary complex
	98	2836.5	1148.0	+4	4588.1	1769.6	2222.8	100	[HexNAc]4[Hex]5[Neu5Ac]1	Biantennary complex
	102	2836.5	1009.3	+5	5041.3	2222.8	2223.7	79	[HexNAc]4[Hex]5[Neu5Ac]1	Biantennary complex
	102	2836.5	1261.6	+4	5042.2	2223.0	1931.5	100	[HexNAc]4[Hex]5[Neu5Ac]2	Biantennary complex
	103	2836.5	1681.5	+3	5041.5	2223.0	2223.0	100	[HexNAc]4[Hex]5[Neu5Ac]2	Biantennary complex
G19	83	3155.5	1014.8	+5	5069.0	1931.5	1931.7	79	[HexNAc]4[Hex]5[Neu5Ac]1	Biantennary complex
	86	3155.5	1073.1	+5	5360.5	2223.0	2222.8	100	[HexNAc]4[Hex]5[Neu5Ac]2	Biantennary complex

^aMonoisotopic mass value.^bRelative peak intensity was calculated by comparing same charge state glycopeptide ions. The intensity of glycoform with maximum intensity at each glycosylation site was considered as 100%.^cThe oligosaccharide composition and type were deduced from its composition.

*The glycopeptides including G16 were found to be oxidized at methionine residue.

When each product ion spectrum of the peptide ions in this LC/ESI MS/MS analysis was identified by the computer program Mascot, the sequence coverage of apoB100 was 38%. The ions, m/z 1177.9 (+3) at 64 min, 1289.0 (+3) at 91 min, and 1053.2 (+3) at 84 min, were identified as TIHDLHLFIENIDFN²²¹²KSGSSTASWIQNVDTK containing the potential *N*-glycosylation site Asn2212 (G7), SSVITLNTNAELFN³³³¹QSDIVAHLLSSSSVIDALQYK containing Asn3331 (G14), and DFHSEYIVSASN⁴⁴⁰⁴-FTSQLSSQVEQLHR containing Asn4404 (G19), respectively (data not shown). These results indicate that some parts of these glycosylation sites were not glycosylated. There were many unexplained peptides and glycopeptides in the digest (data not shown). This may be due to the unexpected digestion or nonspecific cleavage of apolipoprotein B100 as well as the multiple isoforms of the proteins.

LC/ESI MS/MS analysis of chymotryptic digest of apoB100

To determine the carbohydrate at undetected glycosylation sites in the tryptic digest including Asn1341 and 1350 (G4 and G5), which belong to the same tryptic peptide, the chymotrypsin digest was analyzed by LC/ESI MS/MS using the same methodology. Figure 5A shows a TIC of the TOF MS scan for the full scan m/z 700–2000. The collision energy was adjusted at 40–80 eV depending on the precursor ions. A TIC of the product ion scan and extracted ion chromatogram at m/z 204.05–204.15 (HexNAc) are presented in Figure 5B and 5C, respectively.

Figure 6A shows the product ion spectrum of 768.4 (+2) at 14 min for the chymotryptic glycopeptide. The carbohydrate B^+ ions, y_1 and b_2 ions of peptide NW (residue 1341–1342), and peptide + GlcNAc ion were found in the product ion spectrum. The carbohydrate composition, [HexNAc]₂[Hex]₅, was deduced from the calculated carbohydrate molecular ion, 1234.6. Figure 6B shows the product ion spectrum of 1444.1 (+2) at 9 min for the glycopeptide. The carbohydrate B^+ ions, peptide and peptide + GlcNAc ions, and peptide fragment ions from the peptide SGGNT-STDHF (residue 1347–1356) were detected in the product ion spectrum. Carbohydrate molecular weight, 1882.8, was calculated and the oligosaccharide composition, [HexNAc]₂[Hex]₆, was deduced from the molecular weight. The peptide fragment ions were also detected in the product ion spectrum for the chymotryptic glycopeptides as tryptic glycopeptides. The peptide and peptide + GlcNAc ions were detected in product ion spectra. These ions helped us determine the peptide moiety of the glycopeptide ion.

Results of the site-specific analysis of glycosylation of the chymotryptic digest are summarized in Table III. The oligosaccharide heterogeneity at each of 13 *N*-glycosylation sites was determined by LC/ESI MS/MS from the chymotryptic digest of apoB100 (Table III).

Carbohydrate diversity of each site

Results for the tryptic digest and chymotryptic digest of apoB100 are listed in Table IV. The oligosaccharide composition and type were deduced based on the molecular weight and previously reported oligosaccharide structures of apoB100. No information on glycosylation at Asn7 and 2533 (G1 and 8) was obtained from the analysis of the

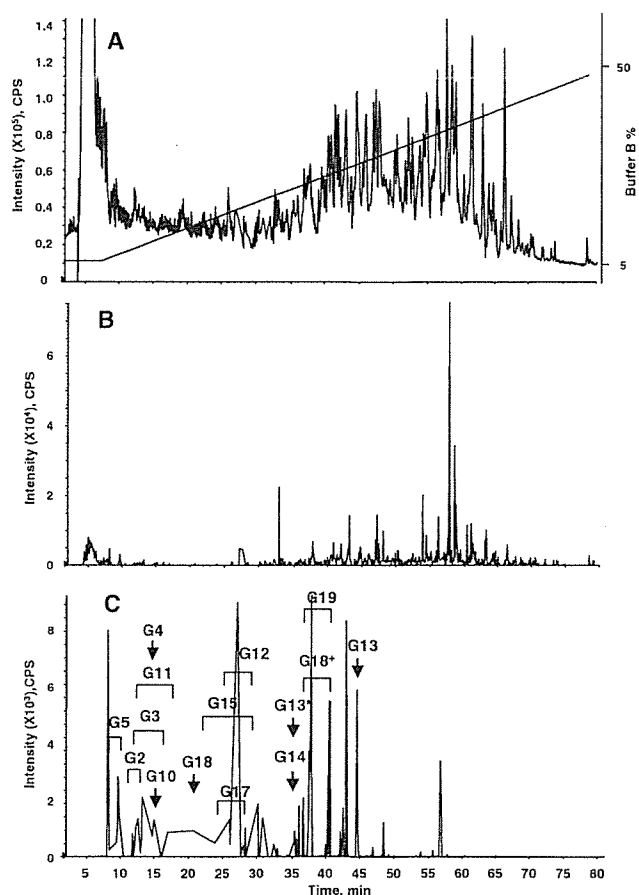


Fig. 5. LC/ESI MS/MS of chymotryptic digest of apolipoprotein B100. TIC of TOF MS scan for the full scan m/z 700–2000 and the HPLC gradient are indicated (A). TIC of the product ion scan data-dependently acquired (B). Extract ion chromatogram at m/z 204 of product ion spectra (C). Arrows and brackets denote glycopeptide fraction and *N*-glycosylation site ID. G13* was found to be oxidized at a methionine residue. G18* was found as missed cleaved glycopeptides.

tryptic or chymotryptic digest. When the tryptic digest of apoB100 was analyzed by LC/ESI MS/MS with the MS range m/z 400–2000, the sequence coverage of apoB100 was 41% and tryptic peptides containing Asn7, 2212, 2533, or 2955 (G1, 7, 8, or 10) were detected (data not shown). Together with the result of LC/ESI MS/MS with the MS range m/z 1000–2000, Asn7 and 2533 (G1 and 8) were not glycosylated or glycosylated only under detection sensitivity, and Asn2212, 2955, 3331, and 4404 (G7, 10, 14, and 19) were partially glycosylated. These findings indicate that 17 of 19 potential *N*-glycosylation sites in apoB100 were glycosylated.

The most heterogeneous oligosaccharides were found at Asn3384 (G15). Asn3384 possessed neutral or monosialylated hybrid and monoantennary complex type and mono- or disialylated biantennary complex type oligosaccharides as well as one high-mannose type oligosaccharide. Asn158, 1341, 1350, 3309, and 3331 (G2, 4, 5, 13, and 14) were occupied by high-mannose type oligosaccharides, whereas Asn956, 1496, 2212, 2752, 2955, 3074, 3197, 3438, 3868,

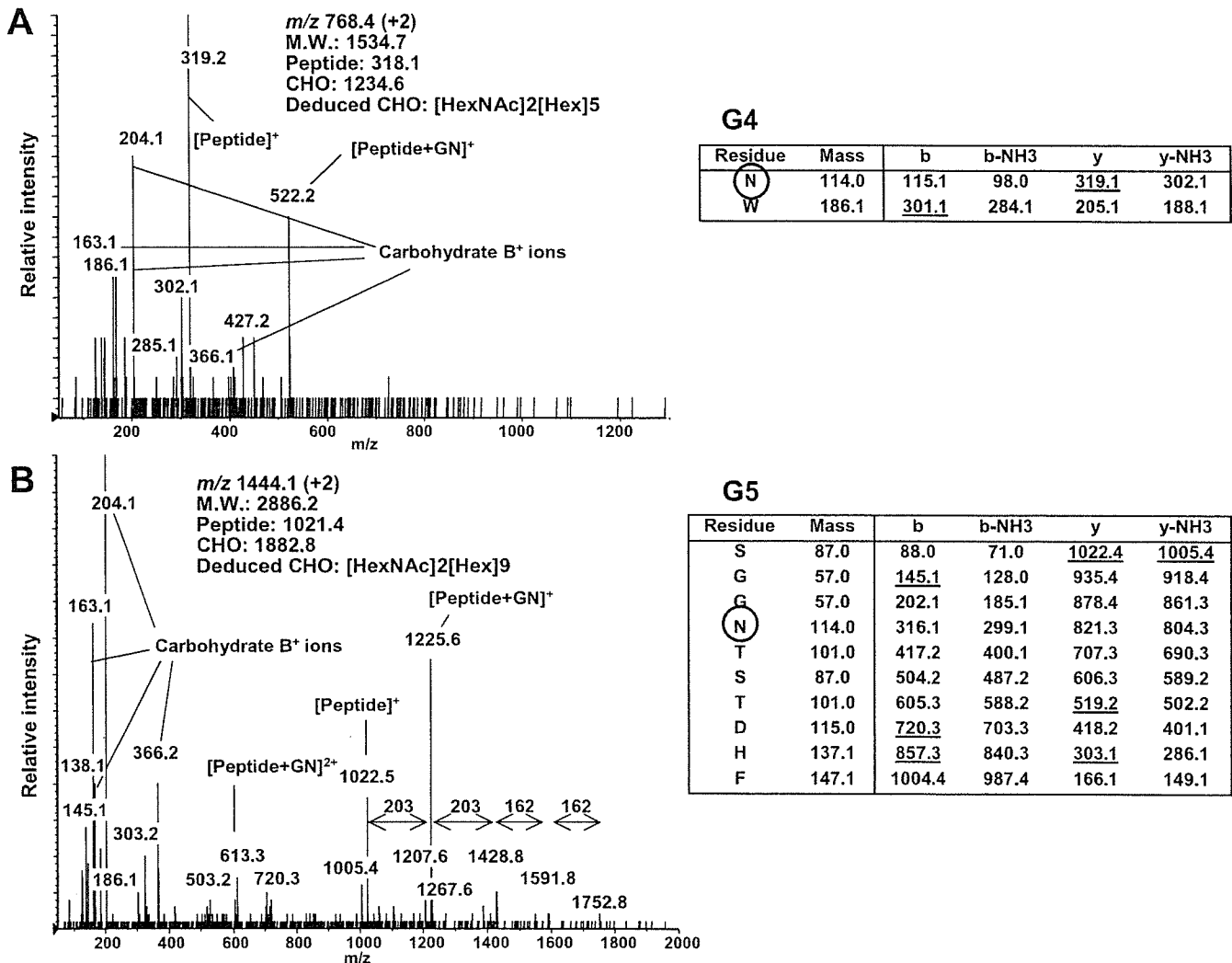


Fig. 6. Product ion spectra of the chymotryptic *N*-glycosylated peptides of apoB100. (A) Product ion spectrum of *m/z* 768.4 (+2) at 14 min for the glycopeptide consisting of residues 1341–1342. Peptide b and y ions of the peptide NW were found. Table shows *m/z* of the proposed b- and y-series fragment ions, and the detected ions are underscored. (B) Product ion spectrum of *m/z* 1444.1 (+2) at 9 min for the glycopeptide consisting of residues 1347–1356. Several ions are consistent with the b- and y-series fragment ions derived from the peptide SGGNTSTDHF. Table shows *m/z* of the proposed b- and y-series fragment ions, and the detected ions are underscored.

4210, and 4404 (G3, 6, 7, 9–12, and 16–19) were predominantly occupied by monosialylated or disialylated biantennary complex type oligosaccharides (Figure 7).

Discussion

Although the role of the carbohydrate structures in LDL and/or apoB100 has been examined in several studies (Attie *et al.*, 1979; Filipovic *et al.*, 1979; Fujioka *et al.*, 2000; Orekhov *et al.*, 1989; Shireman and Fisher, 1979), it is still unknown. It is necessary to elucidate the diversity of the oligosaccharides at each *N*-glycosylation site. This is the first report on the characterization of *N*-linked oligosaccharides in apoB100 at each glycosylation site. The protein was initially carboxymethylated and digested with an enzyme

(trypsin or chymotrypsin), and then the complex mixtures of peptides and glycopeptides were subjected to LC/ESI MS/MS analysis. Product ion scan of each precursor ion was carried out in a data-dependent manner. The glycopeptide molecular ions were easily distinguished from peptide ions by the presence of carbohydrate-related oxonium ions, such as *m/z* 204 (HexNAc), 186 (HexNAc–H₂O), 168 (HexNAc–H₂O), 366 (HexHexNAc), and others in product ion spectra. Furthermore, product ion spectra provided information for the elucidation of the amino acid sequence of the glycopeptides.

The oligosaccharide structure could be deduced based on the calculated molecular weight of the oligosaccharide moiety. The glycopeptide precursor ion was assigned using three strategies. (1) By comparing the product ions of the glycopeptide with the expected fragment ions derived from

Table III. Site-specific glycosylation analysis of the chymotryptic digest of apoB100 using LC/ESI MS/MS

Glycosylation site ID	Retention time (min)	Peptide theoretical MW ^a	Glycopeptides			Oligosaccharide			Relative peak intensity (%) ^b	Composition ^c	Deduced Type ^e
			m/z	Charge	Calculated MW ^a	Calculated MW ^a	Theoretical MW ^a				
G1	—	560.3	—	—	—	—	—	—	—	—	
G2	11	822.3	1344.5	+2	2687.0	1882.7	1882.6	4	[HexNAc]2[Hex]9	High mannose	
	11	822.3	1263.5	+2	2525.0	1720.7	1720.6	7	[HexNAc]2[Hex]8	High mannose	
G3	11	822.3	1182.5	+2	2363.0	1558.7	1558.5	15	[HexNAc]2[Hex]7	High mannose	
	12	822.3	1101.4	+2	2200.8	1396.5	1396.5	12	[HexNAc]2[Hex]6	High mannose	
	12	822.3	1020.4	+2	2038.8	1234.5	1234.4	100	[HexNAc]2[Hex]5	High mannose	
	12	1088.4	1001.8	+3	3002.4	1932.0	1931.7	70	[HexNAc]4[Hex]5[Neu5Ac]1	Biantennary complex	
G4	15	1088.4	1098.8	+3	3293.4	2223.0	2222.8	100	[HexNAc]4[Hex]5[Neu5Ac]2	Biantennary complex	
	14	318.1	768.4	+2	1534.8	1234.7	1234.4	—	[HexNAc]2[Hex]5	High mannose	
G5	9	1021.4	963.1	+3	2886.3	1882.9	1882.6	100	[HexNAc]2[Hex]9	High mannose	
	9	1021.4	1444.1	+2	2886.2	1882.8	—	—	—	—	
G6	9	1021.4	1363.1	+2	2724.2	1720.8	1720.6	40	[HexNAc]2[Hex]8	High mannose	
	9 ^d	1021.4	1282.1	+2	2562.2	1558.8	1558.5	16	[HexNAc]2[Hex]7	High mannose	
G7	—	469.2	—	—	—	—	—	—	—	—	
G8	—	1023.5	—	—	—	—	—	—	—	—	
G9	—	515.3	—	—	—	—	—	—	—	—	
G10	—	2846.4	—	—	—	—	—	—	—	—	
	15	279.1	829.0	+3	2484.1	2223.0	2222.8	—	[HexNAc]4[Hex]5[Neu5Ac]2	Biantennary complex	
G11	15	279.1	1243.0	+2	2484.0	2222.9	—	—	—	—	
	13	521.2	812.7	+3	2435.1	1931.9	1931.7	100	[HexNAc]4[Hex]5[Neu5Ac]1	Biantennary complex	
G12	13	521.2	1218.5	+2	2435.0	1931.8	—	—	—	—	
	16	521.2	909.8	+3	2726.3	2223.0	2222.8	52	[HexNAc]4[Hex]5[Neu5Ac]2	Biantennary complex	
G13	28	878.5	1028.8	+3	3083.4	2222.9	2222.8	—	[HexNAc]4[Hex]5[Neu5Ac]2	Biantennary complex	
	44	978.5	1341.6	+2	2681.2	1720.7	1720.6	31	[HexNAc]2[Hex]8	High mannose	
G13	44	978.5	1260.6	+2	2519.1	1558.6	1558.5	50	[HexNAc]2[Hex]7	High mannose	
	44	978.5	1179.5	+2	2357.1	1396.6	1396.5	100	[HexNAc]2[Hex]6	High mannose	

Table III. continued

Glycosylation site ID	Retention time (min)	Peptide theoretical MW ^a	Glycopeptides		Oligosaccharide			Relative peak intensity (%) ^b	Composition ^c	Deduced Type ^e
			<i>m/z</i>	Charge	Calculated MW ^a	Calculated MW ^a	Theoretical MW ^a			
G14	44	978.5	1098.5	2	2195.0	1234.5	1234.4	75	[HexNAc]2[Hex]5	High mannose
	35 ^d	995.5*	1349.6	+2	2697.1	1719.6	1720.6	16	[HexNAc]2[Hex]8	High mannose
	35 ^d	995.5*	1268.5	+2	2535.0	1557.5	1558.5	49	[HexNAc]2[Hex]7	High mannose
	35	995.5*	1187.5	+2	2373.0	1395.5	1396.5	100	[HexNAc]2[Hex]6	High mannose
	35	995.5*	1106.5	+2	2211.0	1233.5	1234.4	89	[HexNAc]2[Hex]5	High mannose
G15	35	995.5	954.4	+3	2860.3	1882.8	1882.6	—	[HexNAc]2[Hex]9	High mannose
	35	995.5	1431.2	+2	2860.3	1882.8	—	—	—	—
	24	1128.5	1173.5	+2	2345.0	1234.6	1234.4	3	[HexNAc]2[Hex]5	High mannose
	24 ^d	1128.5	1275.0	+2	2548.0	1437.5	1437.5	9	[HexNAc]3[Hex]5	Hybrid
	27	1128.5	1015.1	+3	3042.4	1931.9	1931.7	100	[HexNAc]4[Hex]5[Neu5Ac]1	Biantennary complex
G16	27	1128.5	947.4	+3	2839.3	1728.8	1728.6	79	[HexNAc]3[Hex]5[Neu5Ac]1	Hybrid
	27	1128.5	893.4	+3	2677.3	1566.8	1566.6	23	[HexNAc]3[Hex]4[Neu5Ac]1	Monoantennary complex
	30	1128.5	1112.2	+3	3333.5	2223.0	2222.8	28	[HexNAc]4[Hex]5[Neu5Ac]2	Biantennary complex
	—	550.2	—	—	—	—	—	—	—	—
	28	490.2	899.4	+3	2695.2	2223.0	2222.8	—	[HexNAc]4[Hex]5[Neu5Ac]2	Biantennary complex
G17	28	490.2	1348.5	+2	2695.0	2222.8	—	—	—	—
	21	1082.6	999.8	+3	2996.4	1931.8	1931.7	100	[HexNAc]4[Hex]5[Neu5Ac]1	Biantennary complex
	25	1082.6	1096.8	+3	3287.4	2222.8	2222.8	51	[HexNAc]4[Hex]5[Neu5Ac]2	Biantennary complex
	37	1229.6 [†]	786.9	+4	3143.5	1931.9	1931.7	100	[HexNAc]4[Hex]5[Neu5Ac]1	Biantennary complex
	37	1229.6 [†]	1048.8	+3	3143.5	1931.8	—	—	—	—
G18	38	1229.6 [†]	994.8	+3	2981.5	1769.9	1769.6	14	[HexNAc]4[Hex]4[Neu5Ac]1	Biantennary complex
	40	1229.6 [†]	859.7	+4	3434.6	2223.0	2222.8	67	[HexNAc]4[Hex]5[Neu5Ac]2	Biantennary complex
	40	1229.6 [†]	1145.9	+3	3434.6	2223.0	—	—	—	—
	37	736.4	884.4	+3	2650.3	1931.9	1931.7	100	[HexNAc]4[Hex]5[Neu5Ac]1	Biantennary complex
	37	736.4	1326.1	+2	2650.2	1931.8	—	—	—	—
G19	40	736.4	981.4	+3	2941.2	2222.8	2222.8	94	[HexNAc]4[Hex]5[Neu5Ac]2	Biantennary complex

^aMonoisotopic mass value.^bRelative peak intensity was calculated by comparing same charge state glycopeptide ions. The intensity of glycoform with maximum intensity at each glycosylation site was considered as 100%.^cThe oligosaccharide composition and type were deduced from its composition.^dProduct ion spectra were not acquired. These ions were considered as glycopeptides by the mass differences of 162(Hex) or 203(HexNAc) from the glycopeptides.^eThe glycopeptides including G13 were found to be oxidized at methionine residue.[†]Peptides of these glycopeptides including G18 were found as missed cleaved. The peptide sequence was considered as SKVHN⁴²¹⁰GSEILF.

Table IV. Summary of apoB100 oligosaccharide structure obtained from tryptic digest and chymotryptic digest

Glycosylation site ID	Deduced oligosaccharide composition ^a	Deduced oligosaccharide type ^a
G1	Not glycosylated	—
G2	[HexNAc]2[Hex]9	High mannose
G3	[HexNAc]4[Hex]5[Neu5Ac]1	Biantennary complex
G4	[HexNAc]2[Hex]5	High mannose
G5	[HexNAc]2[Hex]9	High mannose
G6	[HexNAc]2[Hex]5	High mannose
	[HexNAc]3[Hex]7[Neu5Ac]1	Hybrid
	[HexNAc]3[Hex]4[Neu5Ac]1	Monoantennary complex
G7	[HexNAc]4[Hex]4[Neu5Ac]1	Biantennary complex
	[HexNAc]4[Hex]5[Neu5Ac]1	Biantennary complex
	[HexNAc]4[Hex]5[Neu5Ac]1	Biantennary complex
G8	Not glycosylated	—
G9	[HexNAc]4[Hex]5[Neu5Ac]2	Biantennary complex
G10	[HexNAc]4[Hex]5[Neu5Ac]1	Biantennary complex
G11	[HexNAc]4[Hex]5[Neu5Ac]1	Biantennary complex
G12	[HexNAc]4[Hex]5[Neu5Ac]2	Biantennary complex
G13	[HexNAc]2[Hex]8	High mannose
G14	[HexNAc]2[Hex]9	High mannose
G15	[HexNAc]2[Hex]5	High mannose
	[HexNAc]3[Hex]6	Hybrid
	[HexNAc]3[Hex]4[Neu5Ac]1	Monoantennary complex
	[HexNAc]4[Hex]5[Neu5Ac]1[Fuc]1	Biantennary complex
G16	[HexNAc]3[Hex]4[Neu5Ac]1	Monoantennary complex
	[HexNAc]4[Hex]4[Neu5Ac]1	Biantennary complex
	[HexNAc]4[Hex]5[Neu5Ac]1	Biantennary complex
	[HexNAc]5[Hex]6[Neu5Ac]2	Triantennary complex
G17	[HexNAc]4[Hex]4[Neu5Ac]1	Biantennary complex
	[HexNAc]4[Hex]5[Neu5Ac]2	Biantennary complex
G18	[HexNAc]4[Hex]4[Neu5Ac]1	Biantennary complex
G19	[HexNAc]4[Hex]5[Neu5Ac]1	Biantennary complex

^aThe oligosaccharide structure was deduced from the molecular weight and previously reported oligosaccharide structures of apoB100.

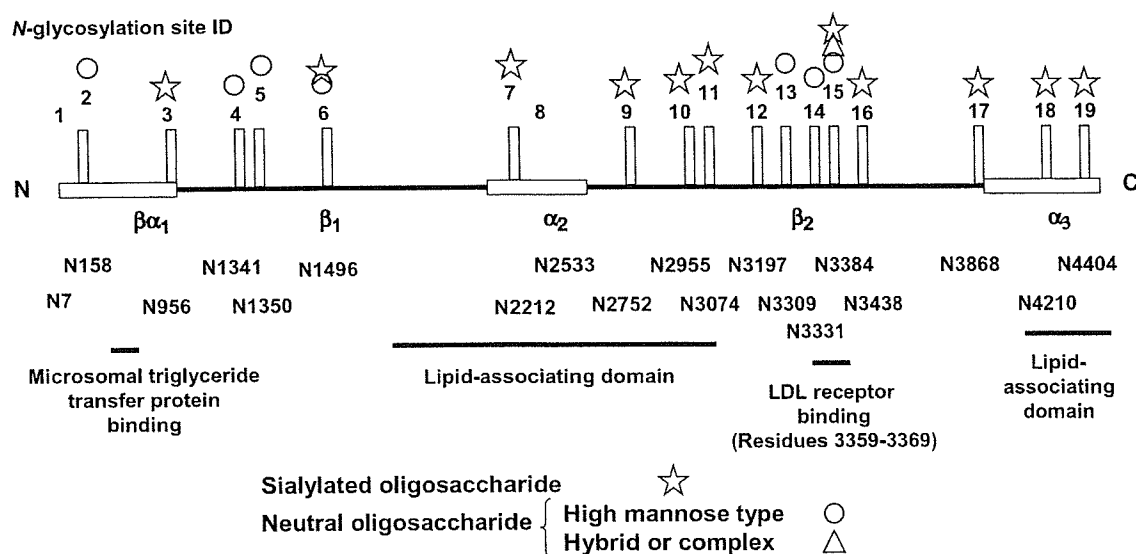


Fig. 7. *N*-glycosylation site of apoB100 and *N*-glycans at each site. *N*-glycosylation sites were shown on the pentapartite structure model, NH₂-βα₁-β₁-α₂-β₂-α₃-COOH, previously reported (Segrest *et al.*, 1994). Circle, triangle, and star indicate high-mannose type oligosaccharides, neutral hybrid or neutral complex oligosaccharides, and mono- or disialylated oligosaccharides, respectively. High-mannose type oligosaccharides were found around the *N*-terminal and near the LDL-receptor binding site, and the other sites were attached by mono- or disialylated oligosaccharides. These oligosaccharide structures may reflect the local 3D structure of VLDL/LDL and may play a biological role.

the peptide containing the *N*-linked glycosylation site, we could directly deduce the peptide moiety. The molecular weight of the oligosaccharide moiety was calculated from the observed molecular weight of the glycopeptide and the theoretical molecular weight of the identified peptide. The carbohydrate composition and structure were deduced from the calculated molecular weight of the oligosaccharide. (2) There were relatively intense peaks of the peptide and peptide + GlcNAc ions in the glycopeptide product ion spectrum. Thus the *m/z* difference of 203 between fragment ions in the product ion spectrum could suggest the molecular weight of the peptide moiety. The peptide was determined from this suggested molecular weight and the molecular weight of the peptides containing the putative *N*-glycosylation site. The molecular weight of the carbohydrate was calculated, and the carbohydrate composition and structure were deduced. (3) Possible glycopeptide masses were calculated from the peptide masses containing the *N*-linked glycosylation site and possible *N*-linked oligosaccharide masses. The possible glycopeptide mass with the measured mass of the glycopeptide was identified. Assignment of peptide moiety was confirmed by the presence of the fragment ions derived from the peptide in the product ion spectrum.

The elution time as well as mass of a glycopeptide is also helpful to elucidate the oligosaccharide structure. The glycopeptides were eluted following reversed-phase high-performance LC based on the peptide and further separated based on the structure of the attached oligosaccharide (Kawasaki *et al.*, 2004). The glycopeptides having the same amino acid sequence were eluted in order of the number of Neu5Ac. Our results show that LC/ESI MS/MS with high sensitivity and high detection resolution is a powerful technique for the site-specific glycosylation analysis of glycoprotein.

Our study revealed that 17 of the 19 potential *N*-glycosylation sites in apoB100 were glycosylated, and the diversity of oligosaccharides at each of these *N*-glycosylation sites was determined. The deduced oligosaccharide structures in the present study were consistent with the structures previously identified in apoB100 (Garner *et al.*, 2001). Asn2212, which was reported to be unglycosylated (Yang *et al.*, 1989), could be glycosylated. The *N*-glycan structures and patterns are very different at each site. Asn158, 1341, 1350, 3309, and 3331 were occupied by high-mannose type oligosaccharides. The other sites except Asn1496 and 3384 (G6 and G15) were predominantly occupied by mono- or disialylated biantennary complex type oligosaccharides, and no neutral oligosaccharides were detected. These sialylated glycans may play an important biological role. Asn1496 and 3384 were occupied by high-mannose, hybrid, and complex type *N*-linked oligosaccharides. Hybrid-type oligosaccharides were found only at these two sites. The oligosaccharides at Asn 3384 are most heterogeneous, and at least 12 different oligosaccharide structures were present. Neutral complex type and neutral hybrid type oligosaccharides were detected only at this site. It is unlikely that this oligosaccharide heterogeneity is due to the fact that the apoB100 used in this study was extracted from the pooled serum of normolipidemic subjects, because no hybrid type oligosaccharides were detected except at Asn1496 and 3384 in this study, and it was reported that the diversity of the oligosaccharides of apoB100 was highly conserved among subjects (Garner *et al.*, 2001; Taniguchi *et al.*, 1989). It may be suggested that the diversity of the oligosaccharides at each glycosylation site was also conserved among subjects.

The relationship between sialylation and LDL-receptor binding has been examined. Desialylation of LDL increased the internalization of LDL by aortic smooth muscle cells

(Filipovic *et al.*, 1979), macrophage (Fujioka *et al.*, 2000) and aortic intimal cells (Orekhov *et al.*, 1989), but had no effect on degradation in hepatocytes (Attie *et al.*, 1979). These findings appear controversial. Asn3309, 3331, and 3384 are located near the LDL-receptor binding site in apoB100 (residues 3359–3369). Our data showed that these glycosylation sites were populated by high-mannose type (at Asn3309 and 3331) or a variety of oligosaccharides, including neutral or sialylated oligosaccharides (at Asn3384). These findings may indicate that sialic acid residues of apoB100 did not play a significant role in LDL-receptor binding and that desialylated LDL might be internalized by another mechanism. Shireman and Fisher (1979) reported that the removal of carbohydrate from LDL did not alter its binding to fibroblasts. Thus the carbohydrate moieties of LDL might not have a significant role in LDL-receptor binding.

The most interesting observation was that the most heterogeneous oligosaccharides were found at the *N*-glycosylation site (Asn3384) nearest to the LDL-receptor binding site. ApoB100 enwraps the VLDL and LDL particle. The C-terminal crosses over near the LDL-receptor binding site and inhibits binding of VLDL to the LDL receptor (Boren *et al.*, 1998). Conversion of VLDL to smaller LDL allows interaction with the LDL receptor. It is likely that the size of the VLDL/LDL particle could affect the 3D conformation around here. Thus the variety of oligosaccharide at Asn3384 may reflect the local 3D conformation of the VLDL particle and accessibility of trimming and glycosyl transferase enzymes.

The procedure described in this article provides an easy and efficient method for the identification of glycosylation sites and oligosaccharide heterogeneity of glycoproteins. Site-specific glycosylation analysis of apoB100 revealed that the diversity of oligosaccharide was distinct at each site. These data provide information to understand the role of oligosaccharides of apoB100 in LDL particles

Materials and methods

Materials

Acetonitrile, formic acid, chymotrypsin, and guanidine hydrochloride were from Wako Pure Chemicals (Osaka, Japan). Tosylphenylalanine chloromethane (TPCK)-treated trypsin was from Sigma (St. Louis, MO). Human apoB100 was purchased from MP Biomedicals (Irvine, CA). This product is derived from pooled human plasma, which is not particularly high-fat plasma. The water used was obtained from a Milli-Q water system (Millipore, Bedford, MA). All other reagents were of the highest quality available.

Reduction and *S*-carboxymethylation of apoB100

ApoB100 (500 µg) was dissolved in 810 µl of 0.5 M Tris-HCl buffer (pH 8.5) that contained 8 M guanidine hydrochloride and 5 mM ethylenediamine tetra-acetic acid. After the addition of 6 µl 2-mercaptoethanol, the mixture was incubated for 2 h at 40°C. Then, 17 mg of monoiodoacetic acid was added, and the resulting mixture was incubated for 2 h at 40°C in the dark. The reaction mixture was applied to a PD-10 column (Amersham Pharmacia Biotech,

Uppsala, Sweden) to remove the reagents, and the eluate was lyophilized.

Enzyme digestion of apoB100

Reduced and carboxymethylated apoB100 was redissolved in 500 µl 0.1 M Tris-HCl buffer (pH 8.0). Half of the reduced and carboxymethylated apoB100 was incubated with 0.02 µg/µl of TPCK-treated trypsin (1:50 w/w) for 2 h at 37°C and the rest was incubated with 0.04 µg/µl of chymotrypsin (1:25 w/w) for 72 h at 37°C. The enzyme digestions were stopped by storing at -20°C before analysis.

High-performance LC of trypsin or chymotrypsin-digested apoB100

Tryptic digest (4 µg, about 8 pmol) and chymotryptic digest (2 µg, about 4 pmol) were analyzed by LC/ESI MS/MS. High-performance LC was performed on a Paradigm MS 4 equipped with a Magic C18 column (0.2 × 50 mm, Michrome BioResources, Auburn, CA). The eluents consisted of water containing 2% (v/v) acetonitrile and 0.1% (v/v) formic acid (pump A) and 90% acetonitrile and 0.1% formic acid (pump B). Trypsin- or chymotrypsin-digested samples of apoB100 were eluted with 5% B for 10 min, followed by a linear gradient from 5% to 70% of pump B in 130 min at a flow rate of 2 µl/min.

ESI Q-TOF MS/MS

MS analyses were performed using a QSTAR Pulsar i quadrupole TOF mass spectrometer (AB/MDS Sciex, Toronto, Canada) equipped with a nano-electrospray ion source. The mass spectrometer was operated in the positive ion mode. The nanospray voltage was set at 2500 V. Mass spectra for MS analysis were acquired over *m/z* 1000–2000 and 700–2000 for tryptic and chymotryptic digests, respectively, and for MS/MS analysis, over *m/z* 100–2000. After every regular MS acquisition, MS/MS acquisition was performed against multiple charged ions. The molecular ions were selected by data-dependent acquiring in the quadrupole analyzer and fragmented in the hexapole collision cell. The collision energy was varied between 40 and 80 eV depending on the size and charge of the molecular ion. All signals were monoisotopically resolved. Accumulation time of spectra is 1.0 and 2.0 s for MS and MS/MS, respectively.

Acknowledgments

We thank Dr. Nishimaki-Mogami for helpful suggestions. This study was supported by a grant-in-aid for Research on Health Sciences focusing on Drug Innovation from the Japan Health Sciences Foundation.

Abbreviations

apoB100, apolipoprotein B100; ESI, electrospray ionization; LC, liquid chromatography; LDL, low-density lipoprotein; MS, mass spectrometry; TIC, total ion chromatogram; TOF, time of flight; TPCK, Tosylphenylalanine chloromethane; VLDL, very low-density lipoprotein.

References

- Attie, A.D., Weinstein, D.B., Freeze, H.H., Pittman, R.C., and Steinberg, D. (1979) Unaltered catabolism of desialylated low-density lipoprotein in the pig and in cultured rat hepatocytes. *Biochem. J.*, **180**, 647–654.
- Boren, J., Lee, I., Zhu, W., Arnold, K., Taylor, S., and Innerarity, T.L. (1998) Identification of the low density lipoprotein receptor-binding site in apolipoprotein B100 and the modulation of its binding activity by the carboxyl terminus in familial defective apo-B100. *J. Clin. Invest.*, **101**, 1084–1093.
- Carr, S.A., Huddleston, M.J., and Bean, M.F. (1993) Selective identification and differentiation of *N*- and *O*-linked oligosaccharides in glycoproteins by liquid chromatography-mass spectrometry. *Protein Sci.*, **2**, 183–196.
- Chen, S.H., Yang, C.Y., Chen, P.F., Setzer, D., Tanimura, M., Li, W.H., Gotto, A.M. Jr, and Chan, L. (1986) The complete cDNA and amino acid sequence of human apolipoprotein B-100. *J. Biol. Chem.*, **261**, 12918–12921.
- Duffin, K.L., Welply, J.K., Huang, E., and Henion, J.D. (1992) Characterization of *N*-linked oligosaccharides by electrospray and tandem mass spectrometry. *Anal. Chem.*, **64**, 1440–1448.
- Filipovic, I., Schwarzmann, G., Mraz, W., Wiegandt, H., and Buddecke, E. (1979) Sialic-acid content of low-density lipoproteins controls their binding and uptake by cultured cells. *Eur. J. Biochem.*, **93**, 51–55.
- Fujioka, Y., Taniguchi, T., Ishikawa, Y., and Yokoyama, M. (2000) Significance of acidic sugar chains of apolipoprotein B-100 in cellular metabolism of low-density lipoproteins. *J. Lab. Clin. Med.*, **136**, 355–362.
- Garner, B., Harvey, D.J., Royle, L., Frischmann, M., Nigon, F., Chapman, M.J., and Rudd, P.M. (2001) Characterization of human apolipoprotein B100 oligosaccharides in LDL subfractions derived from normal and hyperlipidemic plasma: deficiency of alpha-*N*-acetylneuraminyl-lactosyl-ceramide in light and small dense LDL particles. *Glycobiology*, **11**, 791–802.
- Kawasaki, N., Ohta, M., Itoh, S., and Hayakawa, T. (2004) Analyses of glycopeptides and glycoproteins by liquid chromatography-mass spectrometry and liquid chromatography-tandem mass spectrometry. *Methods Mol. Biol.*, **251**, 263–274.
- Knott, T.J., Pease, R.J., Powell, L.M., Wallis, S.C., Rall, S.C. Jr, Innerarity, T.L., Blackhart, B., Taylor, W.H., Marcel, Y., Milne, R., and others. (1986) Complete protein sequence and identification of structural domains of human apolipoprotein B. *Nature*, **323**, 734–738.
- Law, S.W., Grant, S.M., Higuchi, K., Hospattankar, A., Lackner, K., Lee, N., and Brewer, H.B. Jr. (1986) Human liver apolipoprotein B-100 cDNA: complete nucleic acid and derived amino acid sequence. *Proc. Natl Acad. Sci. USA*, **83**, 8142–8146.
- Ling, V., Guzzetta, A.W., Canova-Davis, E., Stults, J.T., Hancock, W.S., Covey, T.R., and Shushan, B.I. (1991) Characterization of the tryptic map of recombinant DNA derived tissue plasminogen activator by high-performance liquid chromatography-electrospray ionization mass spectrometry. *Anal. Chem.*, **63**, 2909–2915.
- Orehov, A.N., Tertov, V.V., Mukhin, D.N., and Mikhailenko, I.A. (1989) Modification of low density lipoprotein by desialylation causes lipid accumulation in cultured cells: discovery of desialylated lipoprotein with altered cellular metabolism in the blood of atherosclerotic patients. *Biochem. Biophys. Res. Commun.*, **162**, 206–211.
- Segrest, J.P., Jones, M.K., Mishra, V.K., Anantharamaiah, G.M., and Garber, D.W. (1994) ApoB-100 has a pentapartite structure composed of three amphipathic alpha-helical domains alternating with two amphipathic beta-strand domains. Detection by the computer program LOCATE. *Arterioscler Thromb.*, **14**, 1674–1685.
- Shireman, R.B. and Fisher, W.R. (1979) The absence of a role for the carbohydrate moiety in the binding of apolipoprotein B to the low density lipoprotein receptor. *Biochim. Biophys. Acta*, **572**, 537–540.
- Taniguchi, T., Ishikawa, Y., Tsunemitsu, M., and Fukuzaki, H. (1989) The structures of the asparagine-linked sugar chains of human apolipoprotein B-100. *Arch. Biochem. Biophys.*, **273**, 197–205.
- Vukmirica, J., Nishimaki-Mogami, T., Tran, K., Shan, J., McLeod, R.S., Yuan, J., and Yao, Z. (2002) The N-linked oligosaccharides at the amino terminus of human apoB are important for the assembly and secretion of VLDL. *J. Lipid. Res.*, **43**, 1496–1507.
- Yang, C.Y., Chen, S.H., Gianturco, S.H., Bradley, W.A., Sparrow, J.T., Tanimura, M., Li, W.H., Sparrow, D.A., DeLoof, H., Rosseneu, M., and others. (1986) Sequence, structure, receptor-binding domains and internal repeats of human apolipoprotein B-100. *Nature*, **323**, 738–742.
- Yang, C.Y., Gu, Z.W., Weng, S.A., Kim, T.W., Chen, S.H., Pownall, H.J., Sharp, P.M., Liu, S.W., Li, H.W., Gotto, A.M. Jr., and Chan, L. (1989) Structure of apolipoprotein B-100 of human low density lipoproteins. *Arteriosclerosis*, **9**, 96–108.

REGULAR ARTICLE

Glycomic/glycoproteomic analysis by liquid chromatography/mass spectrometry: Analysis of glycan structural alteration in cells

Noritaka Hashii, Nana Kawasaki, Satsuki Itoh, Mashashi Hyuga, Toru Kawanishi and Takao Hayakawa

Division of Biological Chemistry and Biologicals, National Institute of Health Sciences, Tokyo

The alteration of glycosyltransferase expression and the subsequent changes in oligosaccharide structures are reported in several diseases. The analysis of glycan structural alteration in glycoproteins is becoming increasingly important in the discovery of therapies and diagnostic markers. In this study, we propose a strategy for glycomic/glycoproteomic analysis based on oligosaccharide profiling by LC/MS followed by proteomic approaches, including 2-DE and 2-D lectin blot. As a model of aberrant cells, we used Chinese hamster ovary cells transfected with *N*-acetylglucosaminyltransferase III (GnT-III), which catalyzes the addition of a bisecting *N*-acetylglucosamine (GlcNAc) to β -mannose of the mannosyl core of *N*-linked oligosaccharides. LC/MS equipped with a graphitized carbon column (GCC) enabled us to elucidate the structural alteration induced by the GnT-III expression. Using 2-D lectin blot followed by LC/MS/MS, the protein carrying an extra *N*-acetylhexosamine in cells transfected with GnT-III was successfully identified as integrin $\alpha 3$. Thus, oligosaccharide profiling by GCC-LC/MS followed by proteomic methods can be a powerful tool for glycomic/glycoproteomic analysis.

Received: September 20, 2004

Revised: April 22, 2005

Accepted: April 22, 2005

Keywords:

2DE / LC/MS / Lectin blotting / Oligosaccharides profiling

1 Introduction

It is common knowledge that approximately 50% of proteins in mammalian cells are glycosylated and that glycans play crucial roles in various biological events including cell recognition [1], adhesion [2] and cell-cell interaction [3]. The alteration of glycosyltransferase expression and subsequent changes in oligosaccharide structures are reported in several diseases, including inherited diseases [4], the progression of

cancer [5] and autoimmune diseases [6–8]. The analysis of glycan structural alteration in glycoproteins is becoming increasingly important in the discovery of therapies and diagnostic markers.

Comprehensive analysis of proteins in a given cellular sample is the most effective means of elucidating the disease mechanism. Simultaneous separation and characterization of proteins by 2-DE and 2-D LC followed by MS have been utilized as the fundamental approaches to proteomic analysis; however, these approaches alone are ineffectual for the elucidation of the glycan structural alteration in glycoproteins. A strategy based on qualitative and quantitative glycomic analysis is necessary for the study of glycosylation-associated diseases.

LC/MS is widely used for glycosylation analysis in glycoproteins. Previously, we demonstrated that LC/MS equipped with a graphitized carbon column (GCC-LC/MS) is a useful means of oligosaccharide profiling and for the structural analysis of carbohydrates [9–12]. Using this method, oligosaccharides, including high mannose, hybrid and complex

Correspondence: Dr. Nana Kawasaki, 1–18–1, Kamiyoga, Setagaya-ku, Tokyo, 158–8501, Japan

E-mail: nana@nihs.go.jp

Fax: +81-3-3700-9084

Abbreviations: CHO, Chinese hamster ovary; CHO-III cells, CHO cells transfected with *N*-acetylglucosaminyltransferase III; dHex, deoxyhexose; GCC, graphitized carbon column; GlcNAc, *N*-acetylglucosamine; GnT-III, *N*-acetylglucosaminyltransferase III; Hex, hexose; HexNAc, *N*-acetylhexosamine; NeuAc, *N*-acetylneuraminic acid; PNGase F, peptide *N*-glycosidase F

types with or without sialic acids, can be separated, and structural information can be obtained from their mass spectra and chromatographic behavior.

Here we propose a strategy for performing glycomic/glycoproteomic analysis based on a combination of GCC-LC/MS and proteomic approaches.

First, GCC-LC/MS is applied to the analysis of oligosaccharide structural alteration in aberrant cells. Chinese hamster ovary (CHO) cells, used as a model of aberrant cells, were transfected with *N*-acetylglucosaminyltransferase III (GnT-III), which catalyzes the addition of bisecting *N*-acetylglucosamine (GlcNAc) to the trimannosyl core of *N*-linked oligosaccharides [13] and is associated with cell adhesion [14] and the suppression of tumor cell metastasis [15–17]. Then, 2-D lectin blotting followed by LC/MS/MS was used to identify the protein in which glycosylation was altered by the expression of GnT-III.

2 Materials and methods

2.1 Cell lines and culture

The CHO cells were obtained from the Japanese Collection of Research Bioresources (Tokyo, Japan). The human GnT-III cDNA was cloned into the pCI-neo vector. The expression vector was transfected into CHO cells with LipofectAMINE plus reagent, according to the manufacturer's instructions. To screen the transformants, the transfectants were cultured with Ham's F12 medium supplemented with 10% fetal calf serum (FCS) and 1 mg/mL G418. After 2 weeks, the colonies were lifted with a micropipette. A high GnT-III-expressing clone was used in succeeding experiments.

The CHO cells and GnT-III-transfected CHO cells (CHO-III cells) were cultured in Ham's F12 medium supplemented with 10% FCS, 100 U/mL of penicillin and 100 µg/mL of streptomycin under a humidified atmosphere of 95% air and 5% CO₂. After harvesting CHO and CHO-III cells, they were rinsed with PBS containing protease inhibitors and 2 mM EDTA.

2.2 Preparation of insoluble and soluble fractions

The insoluble and soluble fractions were prepared from CHO and CHO-III cells using a Mem-PER Eukaryotic Membrane Protein Extraction Reagent Kit (Pierce Biotechnology, P.O., USA). The detergent in these fractions was removed with Detergent-OUT (Geno Technology, M.O., USA) three times. For desalting and degreasing, seven volumes of acetone were added to the sample solution, and the mixture was stirred and sonicated. The mixture was then incubated at –20°C for 1 h and centrifuged at 4°C for 15 min, 15 000 × g. The supernatants were discarded, and the pellets dried. The protein concentrations were determined using a BCA protein assay kit (Pierce).

2.3 Preparation of *N*-linked oligosaccharide alditols

The protein (500 µg) from each fraction was dissolved in 810 µL of 0.5 M Tris-HCl containing 8 M guanidine-HCl and 5 mM EDTA (pH 8.6), and then 6.0 µL of 2-mercaptoethanol were added in the solution. After incubation at room temperature for 2 h, freshly prepared 0.6 M sodium monoiodoacetamide (135 µL) was added to the solution. After incubation at room temperature for 2 h in the dark, the solution was desalted with PD10 column (Amersham Biosciences, NJ, USA), and the elute was lyophilized. The carboxymethylated proteins were dissolved in 500 µL of 100 mM PBS (pH 7.2), and 20 U of peptide *N*-glycosidase F (PNGase F) (Roche Diagnostics, Mannheim, Germany) were added to the solution. After incubation at 37°C for 4 days, 1.74 mL of cold ethanol was added to the solution, the mixture was incubated at –20°C for 3 h, and proteins were removed by centrifugation at 4°C for 10 min (15 000 × g). The supernatants containing oligosaccharides were evaporated, and then lyophilized. The oligosaccharides were incubated with 500 µL of 0.5 M NaBH₄ at room temperature for 16 h, and then neutralized with 10% (v/v) acetic acid to pH 6.5 and desalted with Envi-Carb (Supelco, Bellefonte, USA).

2.4 GCC-LC/MS

LC was carried out using a MAGIC 2002 system (Michrom BioResources, Auburn, CA, USA). The GCC used was a Hypercarb column (150 × 0.2 mm, ThermoFinnigan, San Jose, CA, USA). The eluents were 5 mM ammonium acetate, pH 8.5, containing 2% ACN (pump A) and 5 mM ammonium acetate, pH 8.5, containing 80% ACN (pump B). The borohydride-reduced oligosaccharides were eluted at a flow rate of 2 µL/min with a gradient of 10–45% of pump B in 90 min. Mass spectra were recorded on a TSQ 7000 triple-stage quadrupole mass spectrometer (ThermoFinnigan) equipped with a nanoelectrospray ion source (AMR, Inc., Tokyo, Japan). The mass spectrometer was operated in positive ion mode. Ions in the range of *m/z* 900–2400 were acquired with a scan duration of 3 s. The ESI voltage was set at 2.0 kV, and the capillary temperature was 175°C. The electron multiplier was set at 1.0 kV. Collisions for MS/MS were carried out with collision energy of 25%, scan duration of 4 s., and mass range of *m/z* 100–2000.

2.5 1-D SDS-PAGE and lectin blotting

Proteins were separated by 1-D SDS-PAGE (12.5% T, 3% C) as described by Laemmli [18] and stained with SYPRO Orange (Bio-Rad, Richmond, CA, USA) at room temperature for 30 min in transfer buffer (25 mM Tris-HCl, 20 mM glycine and 20% methanol). The gel images were scanned on a Typhoon 9400 (Amersham Biosciences) at an excitation wavelength of 540/25 nm and an emission wavelength of 590/30 nm. After saving the gel image, the proteins were blotted to a PVDF membrane (Immun-Blot PVDF membrane,

0.2 μm , Bio-Rad) at 3.0 mA/cm², 20 V for 30 min in transfer buffer containing 0.1% SDS using a semi-dry blotter (Transblot SD sel, Bio-Rad). The efficiency and position of the transfer were confirmed using SYPRO Orange transferred together with proteins. Nonspecific sites on the membrane were blocked at 4°C for 16 h in 0.5% casein-PBS. After the membranes were washed with 0.05% Tween-PBS (T-PBS) three times, they were treated with 0.1 U/mL of sialidase (Nacalai Tesque, Kyoto, Japan) at 37°C for 16 h in 0.5 M acetate buffer (pH 5.0). The membranes were then re-blocked with 0.5% casein-PBS at 37°C for 15 min, washed with T-PBS three times, and incubated with biotinylated phytohemagglutinin-E4 (PHA-E4, 2 $\mu\text{g}/\text{mL}$) at 4°C for 2 h in PBS (pH 7.4). The membranes were then washed with T-PBS and incubated with 1:1000 diluted avidin-alkaline phosphatase (AP) complex solution at 4°C for 1 h in PBS.

2.6 Concentration of target proteins in the gel

The band detected by lectin blotting on 1-D gel was excised and then mashed in 20 mM Tris-HCl (pH 8.0) containing 2% SDS. The proteins in the gel particles were extracted by intermittent sonication at 4°C for 30 min, followed by shaking at room temperature for 16 h. After extraction, the gel particles were removed by centrifugation (15 000 \times g). The proteins in the supernatant were precipitated with sevenfold acetone at -20°C for 3 h, and then the precipitates were washed with acetone three times to remove salts and detergent.

2.7 2-DE

For first dimension IEF of the sample, Immobiline DryStrip gel (13 cm, pH4–7 NL, Amersham Biosciences) was used. The samples were dissolved in IEF solution containing 7 M urea, 2 M thiourea, 18 mM DTT, 0.5% IPG buffer, 2% CHAPS, and bromophenol blue. Dried IPG strips were rehydrated overnight in the sample solution. IEF was then performed using the following steps: 500 V for 1 h, 100 V for 1 h, and 8000 V for 2 h, *i.e.* a total of 17.5 kWh.

IPG strips were treated with 10 mL of 50 mM Tris-HCl (pH 8.8) containing 2% SDS, 6 M urea, 30% glycerol and 65 mM DTT for 15 min, and then treated with 10 mL of 50 mM Tris-Cl (pH 8.8) containing 2% SDS, 6 M urea, 30% glycerol and 135 mM iodoacetamide for 15 min in order to reduce the disulfide bonds of cysteinyl residues. SDS-polyacrylamide gels (7.5%T, 3%C, size 140 \times 140 \times 1 mm) and running buffer containing 25 mM Tris-HCl, 192 mM glycine and 0.1% SDS were used for the 2-DE. The gels were run at 25 mA/gel after setting the IPG strip on the gel. Fluorescent staining and scanning of gel, followed by lectin blotting, were performed as mentioned above. In 2-D lectin blotting, the proteins were blotted to a PVDF membrane at 3.0 mA/cm², 20 V for 90 min.

2.8 In-gel digestion and protein identification by LC/MS/MS

Interesting spots were excised from the 2-DE gel for in-gel trypsin digestion. The gel particles were destained with 20 mM ammonium bicarbonate containing 50% methanol in microcentrifuge tubes, and dehydrated in 100% ACN. Enzymatic digestion was performed overnight at 37°C with 5 μL of 20 $\mu\text{g}/\text{mL}$ trypsin (Promega, Madison, WI, USA) in 20 mM ammonium bicarbonate (pH 8.5). Digested peptides were extracted with 1% TFA in 50% ACN, and samples were dried with a Speed-Vac and redissolved in 0.1% TFA for LC/MS.

LC was carried out using a Paradigm MS4 (Michrom BioResources) equipped with Magic C18 column (50 \times 0.2 mm, Michrom BioResources). The eluents were 0.1% formic acid containing 2% ACN (pump A), and 0.1% formic acid containing 90% ACN (pump B). The peptides were eluted at a flow rate of 2 $\mu\text{L}/\text{min}$ with a gradient of 5–70% of pump B in 30 min. Mass spectra were recorded on an API QSTAR Pulsar i (Applied Biosystems, Foster City, CA, USA) in the positive ion mode. The proteins were identified by searching the Swiss-Prot database using MASCOT (Matrix Science, UK). The mass range and MS/MS range were m/z 400–2000 and m/z 100–2000, respectively, and the ESI voltage was set at 2.5 kV.

3 Results

3.1 Analysis of glycans in the insoluble fractions

N-linked oligosaccharides were released from soluble and insoluble fractions by PNGase F and reduced with NaBH₄ to prevent the separation of anomers by GCC. Figure 1A shows the *N*-linked oligosaccharide profile of the insoluble fraction from CHO cells (5×10^7). Diverse oligosaccharide ions were detected by full scan in the positive ion mode of MS. Oligosaccharides were numbered with the labels on peaks where they were detected, and the multiple oligosaccharides in single peak were classified by the digits behind alphabets, such as peaks A1 and A2. Their monosaccharide compositions were deduced from the m/z values as shown in Table 1. *N*-linked oligosaccharides from CHO cells have a high proportion of high mannose-type and bi-, tri- and tetra-antennary complex type oligosaccharides [19, 20]. High mannose-type oligosaccharides, [Man]_{5–9}[GlcNAc]₂ were detected at 9–23 min (peaks A–E and K). Major components (peaks N2, Q2, R1, S1, T1, U1 and V2) were deduced as fucosylated and non-fucosylated biantennary forms with mono- and di-sialic acids from previous articles and their monosaccharide compositions. Various oligosaccharides, including mono- (peak N1 and Q1), tri- (peak P1, U2, V1), tetra-antennary (peak V3), and hybrid-type (peak F1 and I1) oligosaccharides were detected as minor components together with low molecular weight oligosaccharides such as the trimannosyl core (peaks G1 and O1).

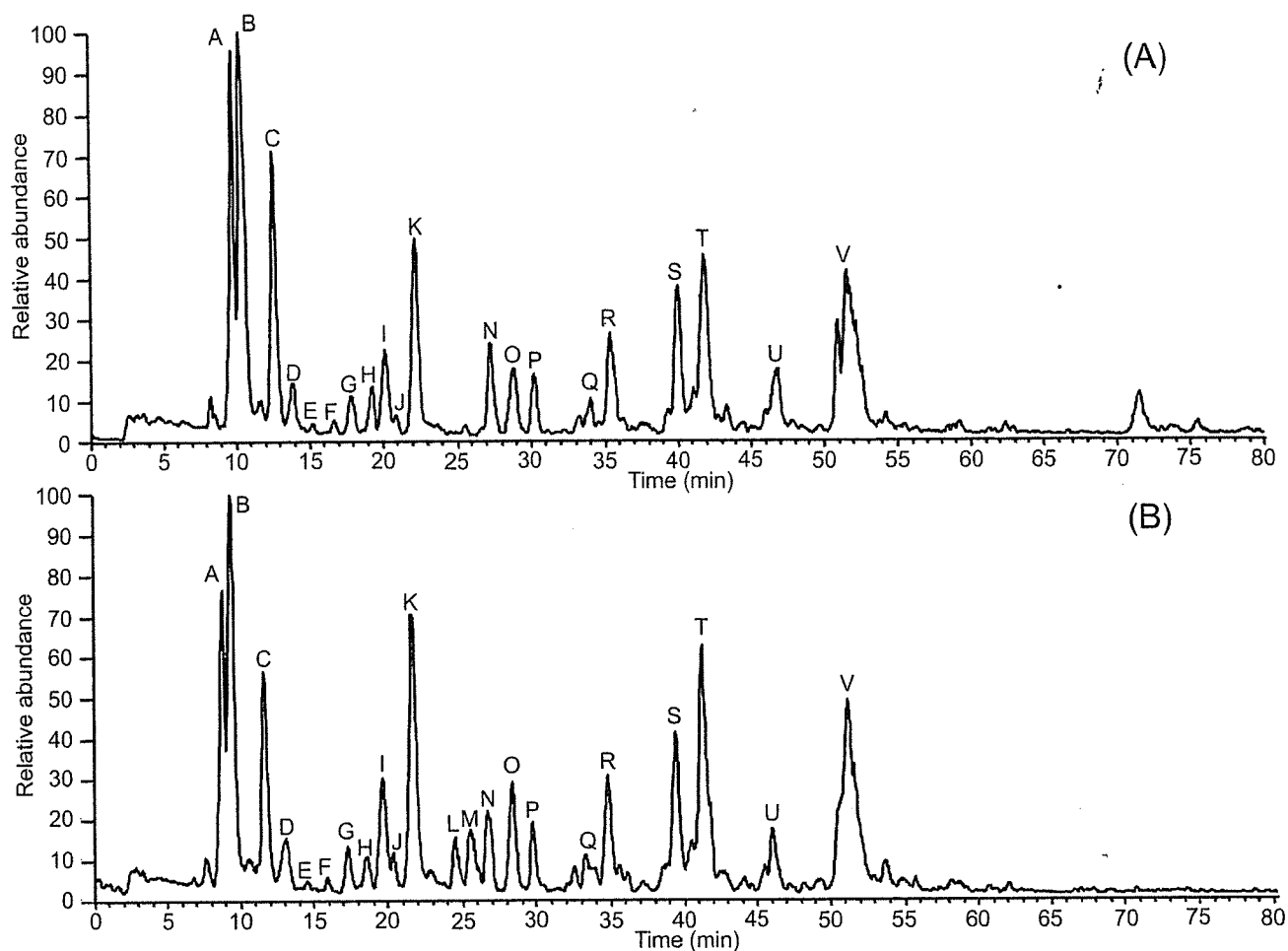


Figure 1. Total ion chromatograms of GCC-LC/MS of borohydride-reduced *N*-linked oligosaccharides released from insoluble fraction of CHO (A) and CHO-III (B) in positive ion mode. Pump A: 5 mM ammonium acetate, pH 8.5, containing 2% ACN. Pump B: 5 mM ammonium acetate, pH 8.5, containing 80% ACN. The borohydride-reduced oligosaccharides were eluted at a flow rate of 2 μ L/min with a gradient of 10–45% of pump B in 90 min.

Figure 1B shows the oligosaccharide profile of the CHO-III-insoluble fraction. The distribution of oligosaccharides in CHO-III was different from that in the CHO cell insoluble fraction. Some additional peaks (peaks L1 and M1) were detected in the CHO-III-insoluble fraction, and their doubly charged ions at m/z 1143.2 and 1143.0 were consistent with the theoretical m/z values of fucosylated biantennary-bearing NeuAc with one additional HexNAc. Figure 2 shows the MS/MS spectrum of peak M1. Detection of B_{17}/Y_6^{2+} at m/z 894.1 and an intense ion of $[\text{HexNAc}]^+$, at m/z 204 suggest that the oligosaccharide (peak M1) carries one GlcNAc at either of the non-reducing ends. Peak M1 is possibly assigned to bisected biantennary form. In addition, peaks D1, I2 and S2, which were not found in the profile of CHO, were detected in that of CHO-III (Fig. 1B). They can also be deduced as bisected biantennary forms from their MS/MS spectra. Other than these oligosaccharides bearing GlcNAc at either of the non-

reducing ends in CHO-III cells, there was no significant difference in glycosylation between CHO and CHO-III cells. These results suggest that only limited oligosaccharides are altered by the expression of GnT-III.

3.2 Analysis of glycans in the soluble fractions

Figure 3A and B shows the *N*-linked oligosaccharide profiles of the soluble fractions of CHO and CHO-III, respectively. The oligosaccharide components of soluble fractions are very different from those of insoluble fractions (Table 1). High mannose-type oligosaccharides, $[\text{Man}]_{5-9}[\text{GlcNAc}]_2$, were detected as major components (peaks A–C and K), and complex-type and hybrid-type oligosaccharides were detected as minor oligosaccharides in the soluble fraction. Oligosaccharides bearing extra GlcNAc (D1, L1 and M1) were also detected in the soluble fraction of CHO-III.

Table 1. Observed *m/z* values and carbohydrate compositions of peaks A-V in total ion chromatogram 3 of CHO-insoluble (Fig. 1A), CHO-III-insoluble (Fig. 1B), CHO-soluble (Fig. 3A) and CHOIII-soluble (Fig. 3B) fractions

Carbohydrate composition ^{a)}	Theoretical mass ^{b)}	Peak No.	Insoluble fraction				Soluble fraction			
			CHO		CHO-III		CHO		CHO-III	
			Charge state	Observed <i>m/z</i>	Charge state	Observed <i>m/z</i>	Charge state	Observed <i>m/z</i>	Charge state	Observed <i>m/z</i>
[Hex] ₇ [HexNAc] ₂	1561.4	A A1	H ⁺	1562.2	H ⁺	1562.0	Na ⁺	1584.4	Na ⁺	1584.2
[Hex] ₈ [HexNAc] ₂	1723.5	A2	Na ⁺	1746.3	Na ⁺	1746.3	Na ⁺	1746.5	Na ⁺	1746.1
[Hex] ₉ [HexNAc] ₂	1885.7	B B1	Na ⁺	1908.4	Na ⁺	1908.5	Na ⁺	1908.4	Na ⁺	1908.9
[Hex] ₆ [HexNAc] ₂	1399.3	C C1	H ⁺	1400.1	H ⁺	1400.0	H ⁺	1399.7	H ⁺	1399.9
[Hex] ₇ [HexNAc] ₂	1561.4	C2	Na ⁺	1584.2	Na ⁺	1584.0	Na ⁺	1584.8	Na ⁺	1584.0
[dHex] ₁ [Hex] ₅ [HexNAc] ₅	1992.9	D D1		N.D. ^{c)}	2H ⁺	997.4		N.D.	2H ⁺	997.5
[Hex] ₆ [HexNAc] ₂	1399.3	D2	Na ⁺	1422.0	Na ⁺	1421.9		N.D.		N.D.
[Hex] ₇ [HexNAc] ₂	1561.4	D3	Na ⁺	1584.2	Na ⁺	1584.1		N.D.		N.D.
[Hex] ₈ [HexNAc] ₂	1723.5	D4	Na ⁺	1746.2	Na ⁺	1746.4		N.D.		N.D.
[Hex] ₄ [HexNAc] ₂	1075.0	E E1	Na ⁺	1097.9	Na ⁺	1097.6		N.D.		N.D.
[Hex] ₆ [HexNAc] ₂	1399.3	E2	H ⁺	1400.1	H ⁺	1400.0		N.D.		N.D.
[Hex] ₆ [HexNAc] ₃	1602.5	F F1	H ⁺	1604.0	H ⁺	1603.1		N.D.		N.D.
[Hex] ₃ [HexNAc] ₂	912.8	G G1	H ⁺	913.7	H ⁺	913.7	Na ⁺	935.7	Na ⁺	935.6
[Hex] ₅ [HexNAc] ₄	1643.5	H H1	H ⁺	1644.5	H ⁺	1644.2	Na ⁺	1666.3	Na ⁺	1666.4
[Hex] ₆ [HexNAc] ₄	1827.6	I I1	2Na ⁺	914.7	2Na ⁺	914.7		N.D.		N.D.
[Hex] ₅ [HexNAc] ₅ [NeuAc] ₁	2137.9	I2		N.D.	2H ⁺	1069.8		N.D.		N.D.
[dHex] ₁ [Hex] ₃ [HexNAc] ₄	1465.4	J J1	H ⁺	1466.1	H ⁺	1466.1	Na ⁺	1488.2	Na ⁺	1487.9
[Hex] ₅ [HexNAc] ₂	1237.1	K K1	H ⁺	1238.0	H ⁺	1238.0	H ⁺	1237.9	H ⁺	1237.9
[dHex] ₁ [Hex] ₅ [HexNAc] ₅ [NeuAc] ₁	2284.1	L L1		N.D.	2H ⁺	1143.2		N.D.	2H ⁺	1142.9
[dHex] ₁ [Hex] ₅ [HexNAc] ₅ [NeuAc] ₁	2284.1	M M1		N.D.	2H ⁺	1143.0		N.D.	2H ⁺	1143.3
[dHex] ₁ [Hex] ₄ [HexNAc] ₃	1424.3	N N1	H ⁺	1425.4	H ⁺	1425.3	Na ⁺	1447.1	Na ⁺	1447.1
[dHex] ₁ [Hex] ₅ [HexNAc] ₄	1789.7	N2	H ⁺	1790.1	H ⁺	1790.3	Na ⁺	1812.3	Na ⁺	1812.1
[dHex] ₁ [Hex] ₃ [HexNAc] ₂	1059.0	O O1	H ⁺	1059.7	H ⁺	1059.7	H ⁺	1059.8	H ⁺	1059.7
[dHex] ₁ [Hex] ₆ [HexNAc] ₅	2155.0	P P1	2H ⁺	1078.5	2H ⁺	1078.5		N.D.		N.D.
[dHex] ₁ [Hex] ₃ [HexNAc] ₃	1262.2	Q Q1	H ⁺	1263.0	H ⁺	1263.0		N.D.		N.D.
[Hex] ₅ [HexNAc] ₄ [NeuAc] ₁	1934.7	Q2	2H ⁺	968.4	2H ⁺	968.4		N.D.		N.D.
[Hex] ₅ [HexNAc] ₄ [NeuAc] ₁	1934.7	R R1	2H ⁺	968.4	2H ⁺	968.4	2H ⁺	968.7	2H ⁺	968.2
[dHex] ₁ [Hex] ₅ [HexNAc] ₄ [NeuAc] ₁	2080.9	S S1	2H ⁺	1041.4	2H ⁺	1041.4	2H ⁺	1041.4	2H ⁺	1041.3
[dHex] ₁ [Hex] ₅ [HexNAc] ₅ [NeuAc] ₂	2574.0	S2		N.D.	2H ⁺	1288.5		N.D.		N.D.
[dHex] ₁ [Hex] ₅ [HexNAc] ₄ [NeuAc] ₁	2080.9	T T1	2H ⁺	1041.4	2H ⁺	1041.5	2H ⁺	1041.4	2H ⁺	1041.3
[Hex] ₅ [HexNAc] ₄ [NeuAc] ₂	2226.0	U U1	2H ⁺	1114.0	2H ⁺	1113.9	2H ⁺	1113.9	2H ⁺	1113.9
[dHex] ₁ [Hex] ₆ [HexNAc] ₅ [NeuAc] ₁	2446.2	U2	2H ⁺	1224.2	2H ⁺	1224.3	2Na ⁺	1124.9		N.D.
[dHex] ₁ [Hex] ₆ [HexNAc] ₅ [NeuAc] ₂	2737.5	V V1	2H ⁺	1370.0	2H ⁺	1370.0		N.D.		N.D.
[dHex] ₁ [Hex] ₅ [HexNAc] ₄ [NeuAc] ₂	2372.1	V2	2H ⁺	1187.1	2H ⁺	1187.1	2H ⁺	1187.2	2H ⁺	1187.2
[dHex] ₁ [Hex] ₇ [HexNAc] ₆ [NeuAc] ₁	2811.6	V3	2H ⁺	1406.8	2H ⁺	1406.6		N.D.		N.D.

The characteristic *m/z* values observed in total ion chromatograms of CHO-III are depicted in bold type.

a) [dHex], deoxyhexose; [Hex], hexose; [HexNAc], *N*-acetylhexosamine; [NeuAc], *N*-acetylneuraminic acid.

b) Monoisotopic mass values.

c) Not detected.